CARACTERIZAÇÃO E CONTROLES DAS MINERALIZAÇÕES AURÍFERAS ASSOCIADAS À SUÍTE GRANÍTICA AURUMINA E FORMAÇÃO TICUNZAL, NO NORDESTE DO ESTADO DE GOIÁS

GABRIEL ANGELO BARBOSA SILVA

Dissertação de Mestrado nº 511

Orientador: Prof. Dr. Nilson Francisquini Botelho

BRASÍLIA – DF

AGOSTO DE 2023

CARACTERIZAÇÃO E CONTROLES DAS MINERALIZAÇÕES AURÍFERAS ASSOCIADAS À SUÍTE GRANÍTICA AURUMINA E FORMAÇÃO TICUNZAL, NO NORDESTE DO ESTADO DE GOIÁS

CHARACTERIZATION AND CONTROLS OF THE GOLD MINERALIZATIONS ASSOCIATED WITH THE AURUMINA GRANITE SUITE AND TICUNZAL FORMATION, NORTHEASTERN GOIAS STATE

GABRIEL ANGELO BARBOSA SILVA

Dissertação de Mestrado apresentada ao Programa de Pós-Graduação em Geologia do Instituto de Geociências da Universidade de Brasília, como requisito parcial obrigatório para obtenção do título de Mestre em Geologia.

Área de concentração: Geologia Econômica e Prospecção

Orientador: Prof. Dr. Nilson Francisquini Botelho

Banca Examinadora:

Prof. Dr. Nilson Francisquini Botelho - Orientador (IG/UNB)
Prof. Dr. Valmir da Silva Souza - Membro interno (IG/UNB)
Prof. Dr. Clóvis Vaz Parente - Membro externo (UFC)

Ficha catalográfica elaborada automaticamente,
com os dados fornecidos pelo(a) autor(a)

Agradecimentos

Agradeço antes de tudo à minha mãe (*in memoriam*), pelo seu amor, que me dá forças para seguir em frente até hoje, por ter me ensinado e encorajado tanto, e pelo seu apoio e incentivo, mesmo relutantes, para que eu fosse para longe em busca do sonho de ser geólogo.

Aos meus irmãos Lorena e Guilherme, que apesar da distância continuaram sempre ao meu lado, me apoiando.

À minha madrinha Simone, pelo acolhimento e carinho.

Agradeço ao professor Nilson, pela orientação, compreensão e confiança, e por todo o aprendizado que recebi desde a graduação.

Aos professores Valmir e Federico pelo auxílio a este trabalho.

À Universidade de Brasília e ao Programa de Pós-Graduação em Geologia do Instituto de Geociências, e aos funcionários do Instituto de Geociências pela colaboração na realização dos trabalhos.

RESUMO

Várias ocorrências de ouro na porção nordeste do Estado de Goiás têm sido esporadicamente exploradas desde o século XVIII. O foco deste trabalho é o estudo dos garimpos Novo Horizonte, Morro dos Borges e Tucano. A região se localiza na parte norte da Faixa Brasília, no seu embasamento paleoproterozoico exposto. As mineralizações de ouro estão relacionadas aos granitos peraluminosos sin-tectônicos da Suíte Aurumina e suas rochas metasedimentares encaixantes da Formação Ticunzal. O minério está hospedado em zonas de cisalhamento com a direção variando de NE-SW até E-W no contato entre biotita-muscovita monzogranito e xisto grafitoso, em muscovita-quartzo milonito derivado do granito. Elementos estruturais e texturais indicam que as mineralizações são concomitantes à deformação dúctil e controladas pela trama S-C, com corpos mineralizados comumente apresentando morfologia sigmoidal, indicadores cinemáticos de rotação dextral e lineação de estiramento mineral oblíqua à foliação. A alteração hidrotermal formou zonas intensamente silicificadas, além de muscovita e clorita hidrotermais, sulfetos e ouro. Sulfetos incluem arsenopirita, pirita, calcopirita, galena, esfalerita e pirrotita. O ouro ocorre livre em veios de quartzo, associado a sulfetos ora como finas inclusões, e como grãos estirados entre lamelas de muscovita. Análises geoquímicas de rocha total em amostras de granito mostram alto SiO_2 e Al_2O_3, enquanto valores de Fe_2O_3 e MgO são mais altos em amostras de xisto. Teores de ouro obtidos alcançam 6.017 ppb em amostra de milonito silicificado de Morro dos Borges, e até 16.273 ppb em veio de quartzo de Novo Horizonte. Amostras de biotita-muscovita granito de Novo Horizonte apresentam concentrações de Pd até 24.2 ppb e de Pt até 14.4 ppb. Amostras de milonito e granito dos depósitos possuem padrões de fracionamento de ETRs similares, e que são menos fracionados do que a média de amostras regionais para granitos da Suíte Aurumina. Dados de microssonda eletrônica em arsenopirita e calcocita de amostras mineralizadas do garimpo de Novo Horizonte indicam enriquecimento em Au, Ni, Co, Se, Bi, Sb e Te, e temperaturas estimadas pelo geotermômetro da arsenopirita entre 390-535 °C são interpretadas como o intervalo de temperatura de cristalização do minério. Razões de $\delta^{34}S$ obtidas por LA-ICP-MS estão entre -1,76 e +5,62‰ para arsenopirita e entre +0,53 e +9,98‰ para pirita de veio mineralizado do depósito de Novo Horizonte. Valores de $\delta^{34}S$ obtidos de sulfeto total dissolvido em minério da

mina de Aurumina foram -4,7‰ para esfalerita, -5,1‰ para pirrotita e -6,4‰ para pirita. Apesar de terem sido classificados como do do tipo ouro orogênico e apresentarem muitas propriedades comuns a este tipo de depósito, as mineralizações possuem características essenciais que são consistentes com depósitos relacionados à intrusões reduzidas. Tais características incluem o ambiente tectônico de interior de arco continental, ocorrência regional de mineralizações de estanho e tungstênio, forte associação com os plútons graníticos, com estruturas ativas durante seu alojamento e resfriamento e precipitação do ouro, e ausência de mineralizações hospedadas no xisto sem a presença de granito. A variação significativa entre valores de $\delta^{34}S$ sugere um componente metasedimentar para a fonte do enxofre, possivelmente incorporada ao magma por contaminação durante sua geração e migração. Um modelo viável para a formação dos depósitos envolve contribuição da Formação Ticunzal durante o transporte do magma, exsolução de fluidos magmático-hidrotermais dos corpos graníticos durante o alojamento controlado pelas zonas de cisalhamento, formando mineralizações hospedadas nas intrusões.

Palavras-chave: Suíte Aurumina; Formação Ticunzal; ouro; intrusion-related; granito peraluminoso; grafita.

ABSTRACT

Various gold occurrences have been sporadically exploited since the XVIII century in the northeast portion of the Goias State, central Brazil, as small-scale and artisanal mines ("*garimpos*"). Study of the *garimpos* named Novo Horizonte, Morro dos Borges and Tucano is the main focus of this work. The region is located in the northern part of the Brasilia Fold Belt, in its exposed Paleoproterozoic basement rocks. The gold mineralizations are related to Paleoproterozoic peraluminous, reduced syn-tectonic granites of the Aurumina Suite, and metasedimentary country rocks of the Ticunzal Formation. The ore is hosted in shear zones, with directions varying from NE-SW to E-W, near the contact between biotite-muscovite monzogranite and graphite-bearing schist, in muscovite-quartz mylonite derived from granite shearing. Structural and textural elements indicate that mineralization is coeval with ductile shearing and is controlled by S-C fabric, with orebodies commonly having sigmoidal morphology with dextral rotation kinematic indicators and oblique mineral stretching lineation. Hydrothermal alteration resulted in intense silicification in narrow zones near the contact between the two lithologies, as well as the crystallization of gold and associated hydrothermal muscovite, chlorite, and sulfides. Ore sulfides include arsenopyrite, pyrite, chalcopyrite, galena, sphalerite, and pyrrhotite. Gold occurs as free grains along fractures in quartz veins, as elongated grains between muscovite lamellae, and as fine inclusions in sulfides. Granite samples in whole-rock chemical analysis have high SiO_2 and Al_2O_3 contents, while Fe_2O_3 and MgO are greater in the schists. Au concentrations obtained from ore samples are up to 6,017 ppb in silicified mylonite from Morro dos Borges, and up to 16,273 ppb in a quartz vein from Novo Horizonte. Biotite-muscovite granite samples from Novo Horizonte have up to 24.2 ppb Pd and 14.4 ppb Pt. Mylonite and granite samples from the deposits show similar REE fractionation patterns, which are less fractionated than those of regional Aurumina granite samples. EPMA results of gold-associated arsenopyrite and chalcocite from the Novo Horizonte deposit indicates variable enrichments in Au, Ni, Co, Se, Bi, Sb, and Te, and arsenopyrite geothermometry temperatures of 390–535°C. Sulfur isotopes LA-ICP-MS spot analysis yelded ranges of $\delta^{34}S$ ratios of -1.76 to +5.62‰ for arsenopyrite and +0.53 to +9.98‰ for pyrite, of a mineralized vein sample from the Novo Horizonte deposit. Bulk dissolved sulfide analysis in ore samples from the Aurumina mine provided $\delta^{34}S$ ratios of -4.7‰ for sphalerite, -5.1‰

for pyrrhotite and -6.4‰ for pyrite. Despite previous classifications as orogenic gold type and having similarities with such deposit type, the mineralizations have some essential features that are also consistent with a reduced intrusion-related gold system classification. Such features include its cordilleran hinterland tectonic environment, a regional association with tin and tungsten mineralizations, a strong association between the ore and the granitic pluton, with structures active during emplacement, cooling, and gold precipitation, high formation temperatures, and absence of mineralizations hosted in schist. The significant variation in $\delta^{34}S$ ratios suggest a metasedimentary component as the source, possibly incorporated to the magma during ascent or at the source. A viable model for the formation of the gold deposits involves contribution from Ticunzal Formation rocks during magma ascent and exsolution of magmatic-hydrothermal fluids from granitic bodies during shear zone-controlled emplacement, in a RIRG system forming intrusion-hosted type mineralizations.

Sumário

Lista de Figuras

Lista de Tabelas

CAPÍTULO 1. INTRODUÇÃO

A região nordeste do Estado de Goiás possui importantes ocorrências de ouro, com vários garimpos e pequenas minas de ouro explorados desde o século XVIII, além de mineralizações de Sn, Ta, U, Ag e EGP, associadas à rochas graníticas da Suíte Aurumina e xistos grafitosos da Formação Ticunzal (Botelho et al., 2006; Botelho et al., 1999; Botelho and Fonteilles, 1992; Botelho and Moura, 1998; Cuadros et al., 2017a; Cunha, 2006; Marini and Botelho, 1986; Menez and Botelho, 2017). As mineralizações de ouro ocorrem na zona de contato entre corpos de granito peraluminoso milonitizado da Suíte Aurumina e pacotes de xisto da Formação Ticunzal. O ouro está hospedado em veios de quartzo e zonas silicificadas contidas em milonito rico em muscovita e quartzo, em zonas de cisalhamento no contato entre as duas unidades.

Este trabalho visa compreender os controles e processos envolvidos na gênese das mineralizações de ouro e o papel das encaixantes como fonte dos fluidos hidrotermais, do ouro e metais associados. A investigação se deu através da caracterização geológica e dos elementos estruturais dos depósitos, geoquímica e caracterização petrográfica do minério e rochas encaixantes, e estudo da química mineral e isótopos de enxofre dos sulfetos associados com a mineralização de ouro, integrando os dados analíticos obtidos com dados de trabalhos realizados na caracterização das rochas da Suíte Aurumina e Formação Ticunzal e outros depósitos de ouro inseridos no mesmo contexto. Na presente pesquisa, foi realizada uma caracterização da mineralização nos garimpos de Novo Horizonte, Morro dos Borges e Tucano, próximos à cidade de Monte Alegre de Goiás (Figura 1). Para realizar uma interpretação de forma universal sobre o sistema mineralizante que gerou esses depósitos, seguiu-se uma abordagem em que se integrou informações levantadas nos trabalhos feitos nas minas de ouro de Aurumina (Cunha, 2006) e Buraco do Ouro (D'el Rey Silva & Senna Filho, 1998; Massucato & Hippert, 1996; Menez, 2014; Menez & Botelho, 2017), os quais possuem as mesmas rochas encaixantes e condições muito semelhantes, com as informações obtidas para os depósitos estudados neste trabalho. Tal entendimento global desses sistemas é uma das justificativas da realização deste trabalho, uma vez que cada depósito havia sido estudado apenas individualmente.

Figura 1. Imagem de satélite da porção nordeste do Estado de Goiás, com a localização dos garimpos de ouro estudados neste trabalho e das minas de Aurumina e Buraco do Ouro.

Especificamente, os objetivos constituíram-se de (i) caracterização da geologia e controle estrutural das mineralizações; (ii) estudo petrográfico das rochas encaixantes e do minério; (iii) caracterização da composição química das rochas encaixantes; (iv) caracaterização da química mineral dos sulfetos presentes no minério; (v) estudo da geoquímica isotópica de enxofre nos sulfetos; (vi) discussão dos processos envolvidos na gênese das mineralizações, possíveis funções específicas desempenhadas pelas rochas encaixantes, e a classificação do tipo de depósito, combinando os dados obtidos e dados da literatura, e (vii) fornecer informações que podem servir de insumos para a exploração na definição de critérios de escolha de áreas potenciais para conter as mineralizações.

A metodologia deste mestrado consistiu inicialmente de uma revisão bibliográfica, durante a qual foram também utilizados dados aerogeofísicos da região dos depósitos, estudados por Serafim (2017), que caracterizou a assinatura aeromagnética e gamaespectrométrica das referidas mineralizações de ouro. Foi realizado um trabalho de campo com visita aos garimpos de Novo Horizonte, Morro

dos Borges e Tucano para descrição das feições geológicas, coleta de amostras e de medidas estruturais. Foram preparadas lâminas delgadas e lâminas polidas no Laboratório de Laminação do Insituto de Geociências da Universidade de Brasília, a partir das amostras coletadas e de algumas amostras coletadas anteriormente em trabalhos finais de graduação em Geologia da universidade.

Foram feitas análises de geoquímica em rocha total em 32 amostras, no ACME Laboratories, Canadá, por ICP-ES e ICP-MS, utilizando digestão multi ácida após fusão com borato de lítio, para elementos maiores e elementos-traço. Foi feita extração por água régia para metais base, e a determinação da concentração de ouro foi feita a partir do método *fire assay*. Elementos maiores foram determinados em termos dos seus respectivos óxidos (SiO_2, TiO_2, Al_2O_3, Fe_2O_3, MnO Cr_2O_3, MgO, CaO, Na_2O, K_2O, e P_2O_5), com resultados expressos em porcentagem em peso. A determinação das porcentagens de enxofre total e carbono orgânico total foram feitas utilizando-se combustão e leitura por infravermelho em LECO. Os elementos-traço analisados foram Be, Cs, Rb, Ba, Sr, Ga, Ni, Co, Cu, Pb, Zn, Ni, Mo, Au, Ag, As, Cd, Sb, Bi, Se, Tl, Hg, Th, U, Zr, Hf, Sn, Nb, Ta, W, V, Sc e ETRs. 7 amostras foram selecionadas ainda para análises de alguns elementos do grupo da platina (Pt, Pd e Rh), realizadas pelo laboratório ActLabs, Canadá, com leituras feitas por meio de Análise por Ativação Neutrônica Instrumental (INAA) e ICP-MS, após fusão por *fire assay*.

Realizaram-se análises de química mineral de arsenopirita (18 análises pontuais) e calcocita (12 análises pontuais) de amostras mineralizadas do garimpo de Novo Horizonte, após metalização por carbono. As análises foram realizadas no Laboratório de Microssonda Eletrônica da Universidade de Brasília, utilizando-se uma microssonda eletrônica da marca JEOL, modelo JXA-8230, acoplada com cinco espectrômetros por dispersão em comprimento de onda (WDS). As condições analíticas utilizadas foram uma voltagem de 20 kV e corrente de 20 nA.

As análises de isótopos de enxofre foram feitas por meio de duas metodologias distintas para amostras provenientes do garimpo Novo Horizonte e da mina de Aurumina, respectivamente. Análises pontuais *in-situ* foram feitas em grãos de arsenopirita (10 análises) e pirita (8 análises) de amostras de veios de quartzo mineralizados do garimpo Novo Horizonte, no Laboratório de Geocronologia da Universidade de Brasília, utilizando-se o equipamento multicoletor LA-ICP-MS Thermo-Finnigan Neptune acoplado a um laser NewWave Nd-YAG 213 nm para

realização das microanálises isotópicas. Análises de isótopos de enxofre de amostras de veio mineralizado de Aurumina foram realizadas em sulfeto dissolvido, com leitura em termos da composição isotópica total de grãos de sulfeto, no caso de esfalerita, pirita e pirrotita. A determinação das composições isotópicas totais foi realizada por meio do espectrômetro de massa Finnigan MAT 251, com voltagem de 10 kV, no Isotope Science Lab, Universidade de Calgary, Canadá.

CAPÍTULO 2. ARTIGO CIENTÍFICO

Genesis of reduced intrusion-related gold deposits associated with the peraluminous Aurumina Granite Suite and Ticunzal Formation schist, central Brazil

Abstract

Gold mineralizations related to Paleoproterozoic peraluminous, reduced syn-tectonic granites of the Aurumina Suite, and metasedimentary country rocks of the Ticunzal Formation are hosted in shear zones near the contact between muscovite monzogranite and graphite-bearing schist. Mineralization is coeval with ductile shearing and is controlled by the S-C fabric. Hydrothermal alteration resulted in intense silicification in narrow zones. Ore sulfides include arsenopyrite, pyrite, chalcopyrite, galena, sphalerite, and pyrrhotite. Gold occurs as free grains along fractures in quartz veins, as elongated grains between muscovite lamellae, and as fine inclusions in sulfides. Granite samples in whole-rock chemical analysis have high SiO_2 and Al_2O_3 contents, while Fe_2O_3 and MgO are greater in the schists. Au concentrations obtained from ore samples are up to 6,017 ppb in silicified mylonite from Morro dos Borges, and up to 16,273 ppb in a quartz vein from Novo Horizonte. Biotite-muscovite granite samples from Novo Horizonte have up to 24.2 ppb Pd and 14.4 ppb Pt. Mylonite and granite samples from the deposits show similar REE fractionation patterns. EPMA results of gold-associated arsenopyrite and chalcocite from the Novo Horizonte deposit indicate variable enrichments in Au, Ni, Co, Se, Bi, Sb, and Te, and arsenopyrite geothermometry temperatures of 390–535°C. Sulfur isotopes LA-ICP-MS spot analysis yelded ranges of $\delta^{34}S$ ratios of -1.76 to +5.62‰ for arsenopyrite and +0.53 to +9.98‰ for pyrite, of a mineralized vein sample from the Novo Horizonte deposit. Bulk dissolved sulfide analysis in ore samples from the Aurumina mine provided $\delta^{34}S$ ratios of -4.7‰ for sphalerite, -5.1‰ for pyrrhotite and -6.4‰ for pyrite. Despite previous classifications as orogenic gold type and having similarities with such deposit type, the mineralizations have some essential features that are also consistent with a reduced intrusion-related gold system classification. Such features include its cordilleran hinterland tectonic environment, a regional association with tin and tungsten mineralizations, a strong association between the ore and the granitic pluton, with structures active during emplacement, cooling, and gold precipitation, high formation temperatures, and absence of mineralizations hosted in schist. The significant variation in $\delta^{34}S$ ratios suggest a metasedimentary component as the source, possibly incorporated to the magma during ascent or at the source. A viable model for the formation of the gold deposits involves contribution from Ticunzal Formation rocks during magma ascent and

exsolution of magmatic-hydrothermal fluids from granitic bodies during shear zone-controlled emplacement, in a RIRG system forming intrusion-hosted type mineralizations.

1. Introduction

Since early the 18th century, gold mineralizations have been intermittently exploited in the northeastern part of Goiás State from small artisanal mines (*garimpos*). The gold mineralizations are related to Paleoproterozoic peraluminous, syn-tectonic granitic intrusions of the Aurumina Suite and its metasedimentary country rocks, a sequence of graphite schists of the Ticunzal Formation. Rocks of the Aurumina Suite also host Sn and Ta mineralizations, while U deposits occur at contacts with rocks of the Ticunzal Formation. The economic potential of this region has made it the subject of numerous studies due to the presence of several deposits of Au, Ag, Sn, Ta, U, Pt, Pd, REEs, In, and gemstones (Botelho et al., 2006; Botelho, 1992; Botelho and Moura, 1998; Marini and Botelho, 1986).

According to Lazarin and Rabelo (1984), small-scale miners (*garimpeiros*) occupied the area near the city of Monte Alegre de Goiás during the 1970s motivated by artisanal mining of gold and cassiterite. This period, however, lasted for little more than 10 years due to the fall in the price of tin, and both gold and tin mining were gradually abandoned. The mines are often privately owned or leased by small cooperatives, with activity that persists up to this day in more recent operations, that include the *garimpos* of Novo Horizonte, Morro dos Borges and Tucano. Due to the artisanal nature of the mining operations, there is no official information available about the Au concentrations and estimated resources. The present work intends to characterize the Au mineralizations at these three locations, to discuss their origin, the conditions necessary for them to form, and the role played by the host rocks in their formation. Additionally, this works intends to integrate these data with informations obtained in previous works carried out on nearby gold deposits that share the same geological context: the gold deposit known as Buraco do Ouro and the Aurumina gold deposit. These deposits occur along the same structural trend and display very similar features (Massucato and Hippert, 1996; D'el Rey Silva L.J.H. and Senna Filho V., 1998; Cunha L.M., 2006; Menez, 2014; Menez and Botelho, 2017).

Therefore, the aim is to describe the mineralizing systems conjointly, with a comprehensive interpretation and discussions over their genesis.

2. Geological setting

The studied region is located in the northern part of the Tocantins Structural Province (Almeida et al., 1981), near to the western margin of the São Francisco Craton, in the external zone of the Brasília Fold Belt (BFB). The BFB was formed during the Neoproterozoic Pan-African/Brasiliano Orogeny following the amalgamation of different lithospheric units through development of large-scale thrust and nappe systems, and strike-slip mega-faults (Fuck, 1994; Fuck et al., 2014; Pimentel et al., 1999; Pimentel and Fuck, 1992; Uhlein et al., 2012). The tectonic subdivision of this part of the belt proposed by Fuck et al. (2014) consists, from west to east, of: i) the Neoproterozoic Goiás Magmatic Arc; ii) the Goias Massif, which includes Archean granite-greenstone terranes as well as Paleo-Mesoproterozoic crystalline basement and Meso-Neoproterozoic volcano-sedimentary sequences; iii) a metamorphic granulitic core of the belt; iv) metasedimentary sequences of the external fold-thrust belt and; v) the exposed basement of the belt represented by the Cavalcante-Natividade crustal block (Fig. 1). The area encompassing the deposits studied in this work lies in the southern portion of the basement that is exposed in the northern sector of the fold belt, in the Cavalcante-Natividade Block. The oldest units in this basement are represented by exposed fragments of granite-gneiss terrains and greenstone belt sequences in the northern portion of this block (Costa and Hasui, 1985; Cruz et al., 2003; Cruz and Kuyumjian, 1998). These units constitute the Almas-Conceição do Tocantins domain (Cruz, 2001; Cruz et al., 2003; Saboia et al., 2020; Sousa et al., 2016), consisting of the 2.2-2.45 Ga Almas-Dianópolis granitic to tonalitic plutons that intruded the Riachão do Ouro greenstone belt sequence of mafic-ultramafic volcanic rocks interbedded with metasedimentary and felsic volcanic rocks (Costa and Hasui, 1985; Cruz and Kuyumjian, 1998; Kuyumjian et al., 2012). The southern portion of the block is mostly composed of the Aurumina suite peraluminous metagranites and the Ticunzal Formation graphite-bearing schists and paragneisses, making up the Cavalcante-Arraias domain (Cordeiro and Oliveira, 2017; Fuck et al., 2014). The Cavalcante-Natividade Block is regarded as the exposed westernmost part of the São Francisco paleo-plate, reworked during the

Neoproterozoic (Brito Neves, 2011; Cordani et al., 2000; Cordani and Sato, 1999; Fuck et al., 2008).

The development of a short-lived arc-related basin during the Rhyacian, and subsequent amphibolite-facies metamorphism, gave origin to the schists and paragneisses of the Ticunzal Formation (Cuadros et al., 2017b). At 2.15-2.16 Ga, a large volume of peraluminous magma constituing the Aurumina suite was emplaced, hosted by rocks of the Ticunzal Formation (Botelho et al., 1999; Cuadros et al., 2017a). After these orogenic events, the Araí Rift was developed, with associated 1.77 Ga tin-bearing A-type granites of the Pedra Branca Suite, and the deposition of the volcanic-sedimentary sequences of the Araí Group, partially covering the older Paleoproterozoic rocks (Botelho and Fonteilles, 1992; Pimentel et al., 1991). Intrusion of tin-bearing granites of the Serra da Mesa Suite at ~1.58 Ga occurred during a later anorogenic magmatic event (Pimentel et al., 1999, 1991). Their Sn mineralizations, together with those associated with granites of the Pedra Branca and Aurumina suites, collectively make up part of the Goiás Tin Province (Marini and Botelho, 1986). The Neoproterozoic Brasiliano tectono-magmatic events affected the Paleo- and Mesoproterozoic basement rocks to varying degrees, and were also responsible for the juxtaposition of the Paleoproterozoic basement next to the younger metasedimentary rocks of the Paranoá and Bambuí groups, deposited in passive margin (southern portion) and foreland basin (eastern portion) settings, respectively (Fuck et al., 2014; Pimentel et al., 1999).
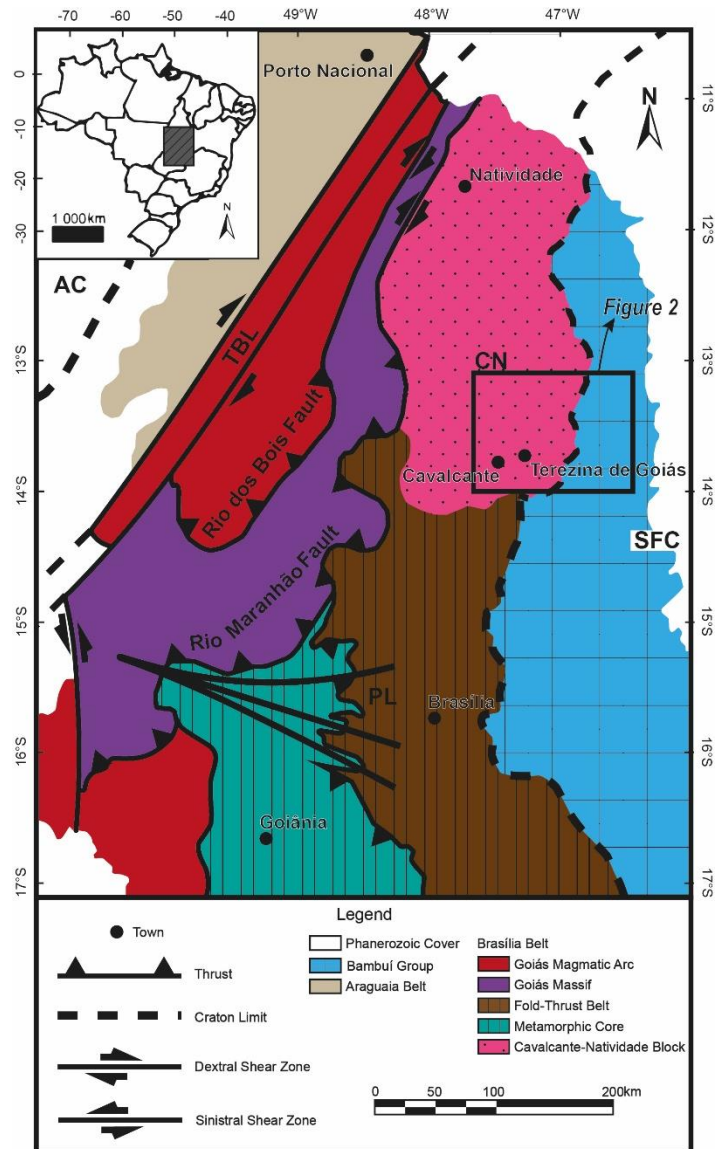
Figure 1. Regional geological map of the BFB. After Fuck et al., 2014. CN: Cavalcante-Natividade block; SFC: São Francisco craton; TBL: Trans-Brasiliano Lineament; PL: Pirineus Lineament; AC: Amazonian Craton.

Ticunzal Formation

The Ticunzal Formation consists of a metasedimentary sequence composed mainly of graphite-bearing schists and paragneisses, with up to 200-300 m in thickness that outcrop as narrow strips 1–2 km wide (Fig. 2) (Alvarenga et al., 2007; Fernandes et al., 1982; Marini et al., 1984, 1978). Metamorphic assemblages of middle-amphibolite facies are observed in these rocks, with relicts of garnet and abundant lamellae of high-temperature graphite (~630ºC; Cuadros et al., 2017b). Nevertheless, a greenschist retrograde paragenesis predominates, composed mainly of biotite, muscovite, and chlorite. The protolith consisted of argillaceous and organic

matter-rich sediments. Sedimentation would have taken place in the 2.16 to 2.19 Ga range as constrained from U-Pb zircon data and field relations with rocks of the Aurumina suite. Older basement granite-gneiss and greenstone sequence mafic-ultramafic rocks from the Almas-Dianópolis terrane have been proposed as possible provenance sources (Cuadros et al., 2017b).

Aurumina suite

Rocks of the Aurumina suite constitute an extensive domain of peraluminous intrusions of granitic and tonalitic/granodioritic composition, hosted by schists and paragneisses of the Ticunzal Formation (Botelho et al., 1999). While the association of peraluminous rocks corresponding to this suite was mapped in detail in the southern portion of the Cavalcante-Natividade block (Alvarenga et al., 2007; Campos et al., 2010), its northern limits are poorly known. However, intrusion of peraluminous granites within metaluminous orthogneisses of the Almas-Conceicão do Tocantins domain has been reported (Corrêa et al., 2015; Oliveira et al., 2012), along with gold mineralizations hosted by those units. The Aurumina Suite plutons have a syn-tectonic character, commonly displaying a mylonitic foliation concordant with the regional N10º-30 ºE mylonitic foliation observed in the host rocks (Botelho et al., 2006). Late facies of this suite, however, show little to no deformation at all. The Aurumina Suite rocks are medium- to coarse-grained, and composed mainly of quartz, microcline, plagioclase, muscovite, and/or biotite, with ilmenite, apatite, zircon, monazite, thorite and garnet as accessory minerals (Botelho et al., 1999). Geochemical data indicate aluminum saturation index >1, high TiO_2 (0.8-1.5 wt.%) in igneous muscovite and highly fractionated REE patterns (Botelho et al., 2006). The Aurumina suite represents a predominantly peraluminous magmatism, which appears associated with coeval intermediate to mafic metaluminous rocks. This association, along with a transitional geochemical character between I- and S-type magmas is thought to be the result of hybridization by reaction between basaltic melts and supracrustal metasedimentary rocks at relatively shallow (<5 km) crustal depths. Such metasedimentary component could be related to rocks that were also source of the 2.2-2.4 Ga Almas-Dianópolis granites and tonalites (Cuadros et al., 2017a). These characteristics, along with the presence of a large volume of tonalitic and granodioritic rocks and a regional correlation with volcanic arc-related rocks of

similar age, led Cuadros et al., (2017a) to suggest a continental arc hinterland tectonic setting for this suite, analogous to the belt of peraluminous granites in the hinterland of the North American Cordillera (Miller and Barton, 1990). In addition to gold, peraluminous granites of the Aurumina Suite also host Sn and Ta deposits related to greisen and LCT-type pegmatites and albitites of later, highly-evolved magmatic phases (Botelho et al., 1999; Botelho and Moura, 1998; Kuyumjian et al., 2012; Sirqueira, 2014).
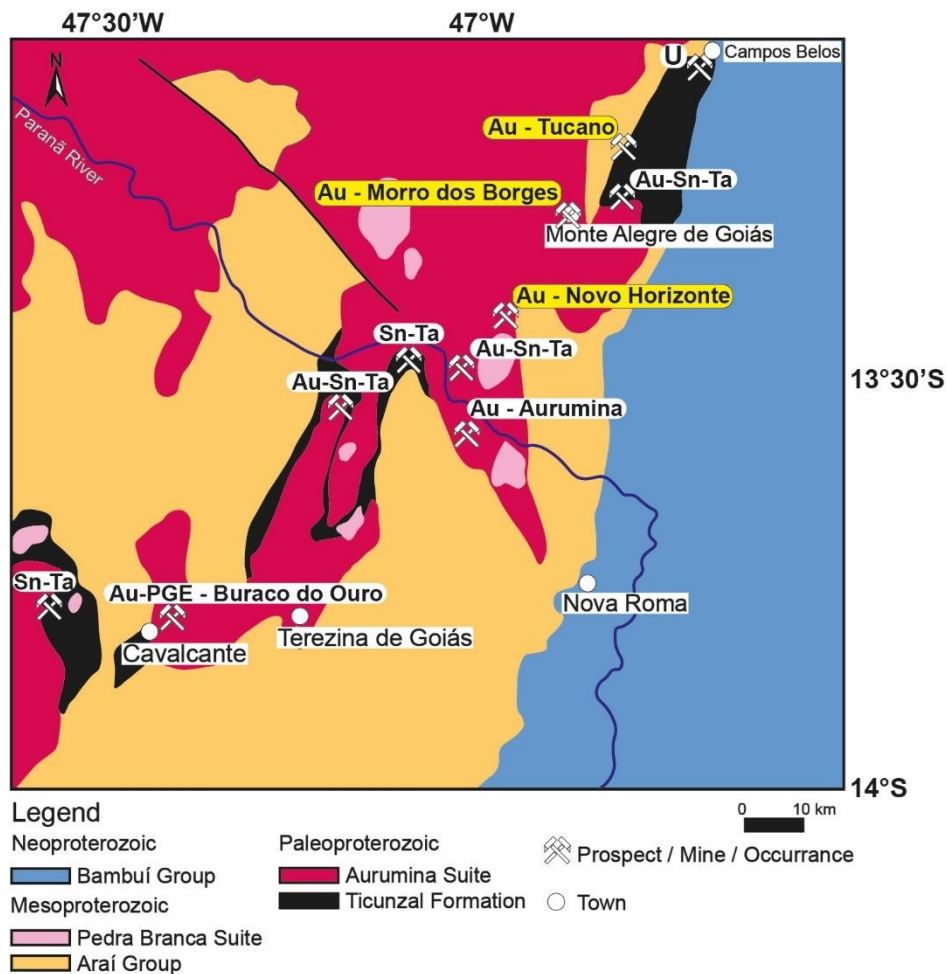
Figure 2. Simplified geological map of the southern portion of the Cavalcante-Natividade block, displaying the locations of ore deposits associated with the Aurumina suite and the Ticunzal Formation. The locations of the deposits studied in this work are highlighted in yellow.

3. Geology of the gold deposits

All of the gold mineralizations mentioned above are hosted in mylonitic rocks at the contact zone between granite and graphite schist. The Morro dos Borges, Novo

Horizonte and Tucano deposits (Fig. 2) are hosted by muscovite-quartz mylonite in NW-W dipping steep to sub-vertical dextral shear zones developed at the contact between muscovite granite of the Aurumina Suite and graphite schist of the Ticunzal Formation (Fig. 5). The shear zones follow a regional NE-SW to NNE-SSW trend in these three deposits, stretching a few tens of kilometers. Further south, shear zones vary from almost N-S directions near the Aurumina deposit, to E-W directions in Cavalcante. The morphology of mineralized zones is intimately associated with mylonitization-related ductile deformation. The degree of grain-size reduction decreases progressively over a narrow zone of 20-30 meters, ranging from ultramylonite to finely foliated granite contaning meter-wide domains of protomylonite. The ore is found in intensely silicified meter-thick zones within the mylonite, typically with terminations that pinch out along their lengths. Field evidence indicates that the silicified zones commonly have slightly undulating geometries in the Morro dos Borges and Novo Horizonte deposits. The geometry of mineralized zones is controlled by a penetrative curviplanar foliation that is oblique to the shear zone strike, forming meter-wide structures with arched ends and sigmoidal morphology. The foliation parallel to the orebodies is the S foliation of the S-C framework developed during shearing, as suggested also by D'el Rey-Silva and Senna Filho (1998) for the Cavalcante deposit. The S foliation displays moderate to steep dip (45° to 75°) with directions varying from N50W to N-S in Morro dos Borges, N30W to N10E in Novo Horizonte, and N10-20E at the Buraco do Ouro deposit (Menez, 204), the latter associated with a E-W shear zone. At Novo Horizonte, however, silicified mineralized zones parallel to the main N10W foliation, which is cross-cut by the S foliation, are also observed, with evidence of brecciation. Lineation defined by mineral striae in C surfaces at Morro dos Borges and Novo Horizonte deposits plunges moderately to NW, with an average N10E direction of the C surface, indicating oblique slip. Mineralization also occurs in quartz veins sub-parallel to the C planes. At the Tucano deposit, gold occurs in the silicified contact zone, and in 10-20 cm wide, subvertical quartz veins (Fig. 5D), sub-parallel to the N40E-striking C foliation. In the Aurumina deposit, mineralizations are concentrated in C foliation-parallel quartz veins, 30 cm to 2 m wide, with lateral continuity up to 250m (Cunha, 2006). These veins commonly display brecciation features, suggesting a prevalence of late, brittle deformation as a structural control of this deposit, with remobilization of

Au and Ag occurring together with quartz and carbonate infill in fractures, and coarse-grained euhedral sulfides not reported in the other deposits.
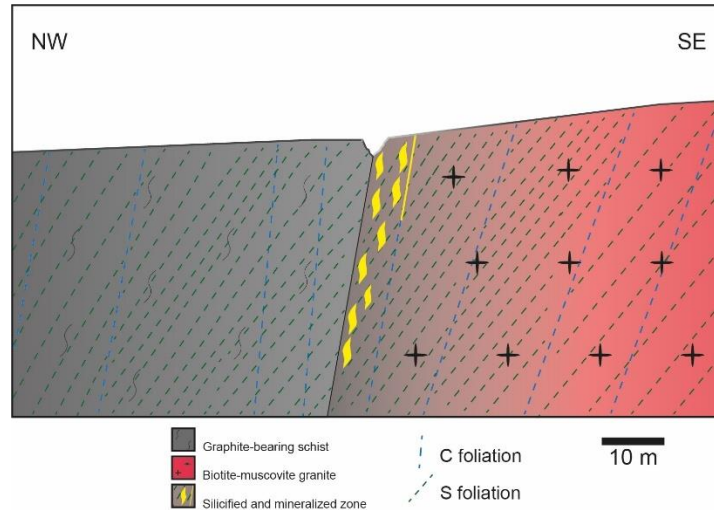
Figure 3. Schematic NW-SE profile along the Novo Horizonte deposit.

3.1. Magnetic and radiometric signature

Previous work aiming to characterize the gold mineralizations associated with the Aurumina suite and Ticunzal Formation using airbone geophysical data of the area of the deposits (Serafim, 2017), attempted to model the structural framework and relate it to the main mineral occurrences in the region, revealing common sigmoidal lineaments 5 to 10 km long, limited by E-W lineaments (Fig. 4). Depth estimation inferred from the Euler deconvolution magnetometric product indicate a greater extension of the shear zones at subsurface, with significant correlation between sigmoidal magnetic features at intermediate depths (approximately 300 m to 1.2 km) and features found at surface. These observations also emphasize the importance of the NE-SW structures at greater depths, and therefore their role as major fluid conduits. Two major NE-SW magnetic features were identified along magnetic profiles based on inferred magnetic susceptibility at depth; they are located 15-20 km apart from each other and define an alignment strip for the deposits. These structures were interpreted as the limits of a major shear zone.
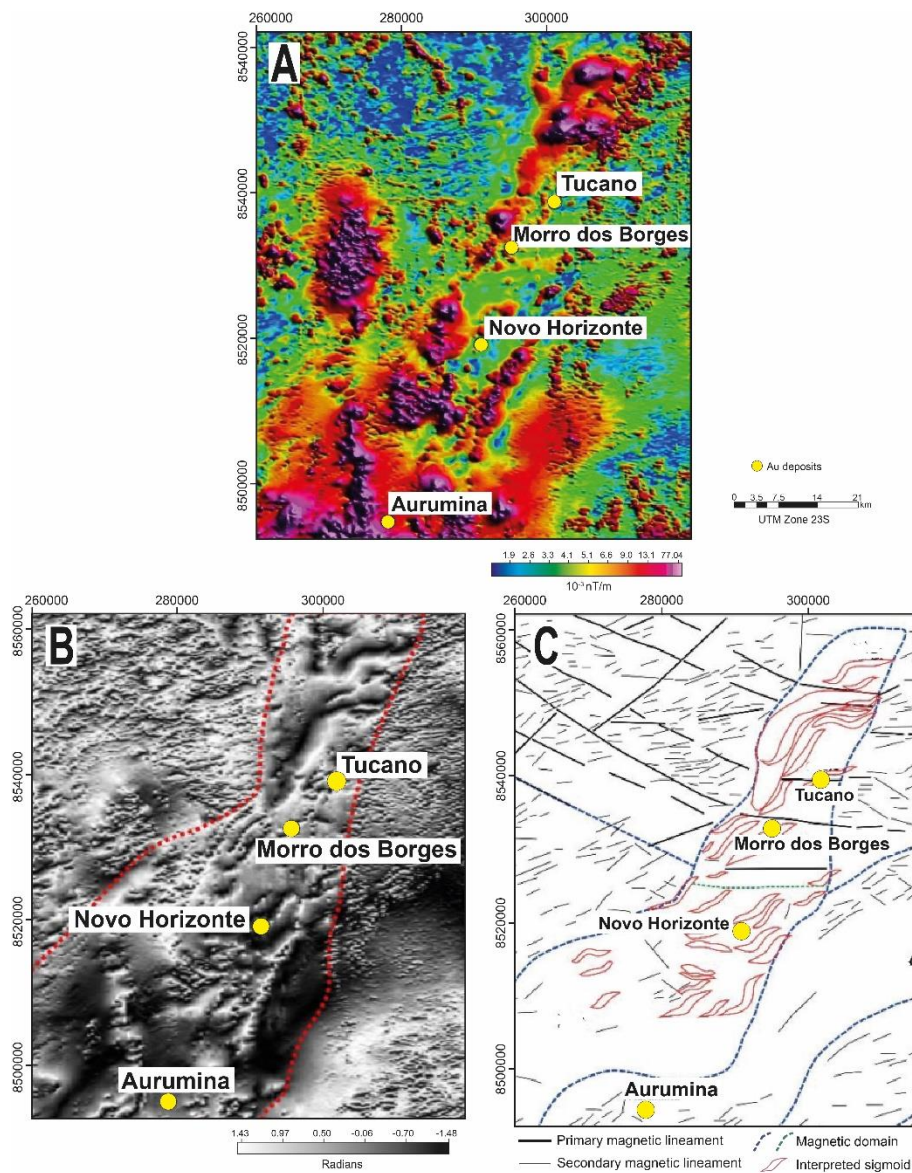
Figure 4. A. Image of the analyitical signal amplitude data for the area of the deposits. The deposits are aligned with NE-striking magnetic anomalies. B. Image of the analyitical signal inclination data. C. Interpretation of magnetic lineaments from the analyitical signal inclination image.

Radiometric data show zones of higher potassium and uranium concentration in relation to thorium (parameter F=K.eU/eTh). These areas coincide with contact zones between the Ticunzal Formation schists and granites of the Aurumina Suite, where there is relevant K enrichment attributed to hydrothermal alteration. The Tucano and Morro dos Borges deposits show anomalous values in both K_d and eU.

However, no anomalous K_d and Ud values were identified in the Novo Horizonte deposit.

3.2. Rock types

3.2.1 Schist

Chlorite-biotite-muscovite-quartz schist is the most common rock type of the Ticunzal Formation occurring in the deposits. In portions of the schist that are more preserved from shearing and hydrothermal alteration, the rocks are dark grey, fine-grained with a granolepidoblastic texture, generally composed of up to 5% graphite, with variable amounts of quartz (30 - 45%), muscovite (20 - 40%), biotite (5 – 15%), chlorite (5 – 15%), and subordinate garnet (5%) and plagioclase (<5%). Rutile, tourmaline, titanite, monazite, and fluorite occur as accessory minerals. Muscovite and chlorite occur as very common retrograde and hydrothermal alteration-related minerals.

Foliation is characterized by a steeply-dipping anastomosing schistosity, with submillimetric parallel intercalation of mica-graphite domains and quartz segregations. Medium-grained quartz crystals and segregations (1-2 mm) often form sigmoidal porphyroblasts, and graphite and mica lamellae form open folds and crenulation cleavage. Coarse muscovite lamellae occur both parallel to the foliation and as aggregates without preferred orientation. Very fine-grained muscovite and quartz form a pervasive alteration groundmass interspaced between coarser-grained domains. Biotite is partially replaced by chlorite, and often displays intergrowths with graphite that form elongated, foliation-parallel lenses with no internal preferred orientation of the minerals, also commonly rich in coarser-grained muscovite. Garnet crystals are replaced by very fine-grained quartz and muscovite forming euhedral medium-grained pseudomorphs, which are commonly strongly deformed. Sheared, mylonitic schist has porphyroblastic sigmoidal garnet, commonly replaced by fine-grained sericite and quartz with coarser muscovite, graphite, and chlorite commonly occurring along shadow pressure zones. Close to the mineralized zones, the graphite schist host rocks display finer grain size, and are either strongly silicified or enriched in graphite, which occurs associated with sericite and coarser hydrothermal muscovite (Fig. 6F). Graphite-bearing microshear bands occur subparallel to schist

foliation, and cut across that foliation on the millimetre scale. Graphite lamellae locally form an intergrowth fabric with muscovite and quartz.
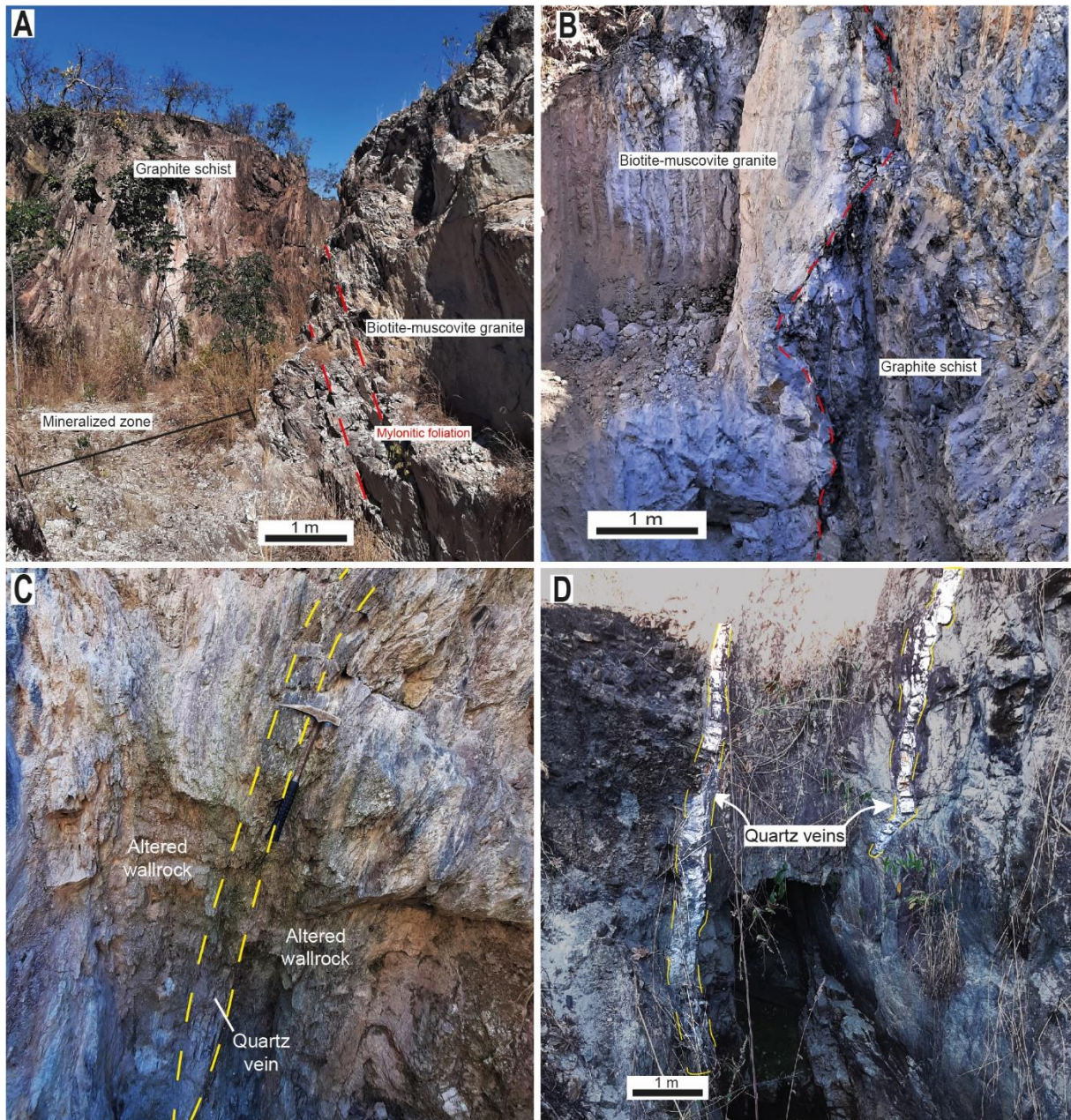
Figure 5. A and B: Photographs of the contact zone between the Ticunzal Formation schist and the Aurumina Suite granite in the Morro dos Borges deposit. C. Mineralized quartz vein and surrounding sericite-chlorite altered wall rock in Morro dos Borges. D. View of the mineralized contact zone at Tucano containing subvertical foliation-parallel quartz veins.

3.2.2 Biotite-muscovite granite

The least-altered granitic rocks in the area of the deposits correspond to greyish white monzogranites, which are medium to fine-grained, foliated, and display a main mineralogical assemblage composed of quartz, plagioclase, perthitic microcline, muscovite, and biotite. Accessory minerals include ilmenite, zircon, apatite, monazite and tourmaline. Quartz and feldspar crystals generally have similar sizes, around 0.5 to 1 mm. Magmatic muscovite occurs as lamellae with the same size to slightly larger than quartz and feldspar crystals (0.5 to 1.5 mm), with sharp, planar grain boundaries forming an interlocking texture with adjacent crystals (Fig. 6B). Feldspar crystals are partially replaced by fine-grained muscovite, with variable degrees of alteration. Incipient alteration forms consumed, serrated grain boundaries and submilimetrical mica-filled microfractures along cleavage and twinning planes, while complete substitution forms a sericitic groundmass that envelops the remaining grains.

Alteration in the granitic rocks is intimately related to deformation. The development of a mylonitic foliation is associated with replacement of original minerals in these rocks by a fine-grained quartz-muscovite matrix, as well as the reduction in grain size and stretching of quartz and (magmatic) muscovite crystals during mylonitization, forming recrystallized quartz and muscovite porphyroclasts, quartz ribbons, a very fine micaceous groundmass, and mica-fish features. Most of the magmatic texture has been obliterated by ductile shearing, producing mylonitic rocks with porphyroclastic recrystallized relicts of quartz, feldspar and muscovite surrounded by a fine-grained groundmass of quartz and muscovite (Fig. 7A). Even though some mylonite is composed mainly of quartz and fine-grained muscovite, few remnants of potassium feldspar and fragments of magmatic muscovite crystals can be identified in thin section, suggesting that this mylonite was formed by shearing of granitic rocks.
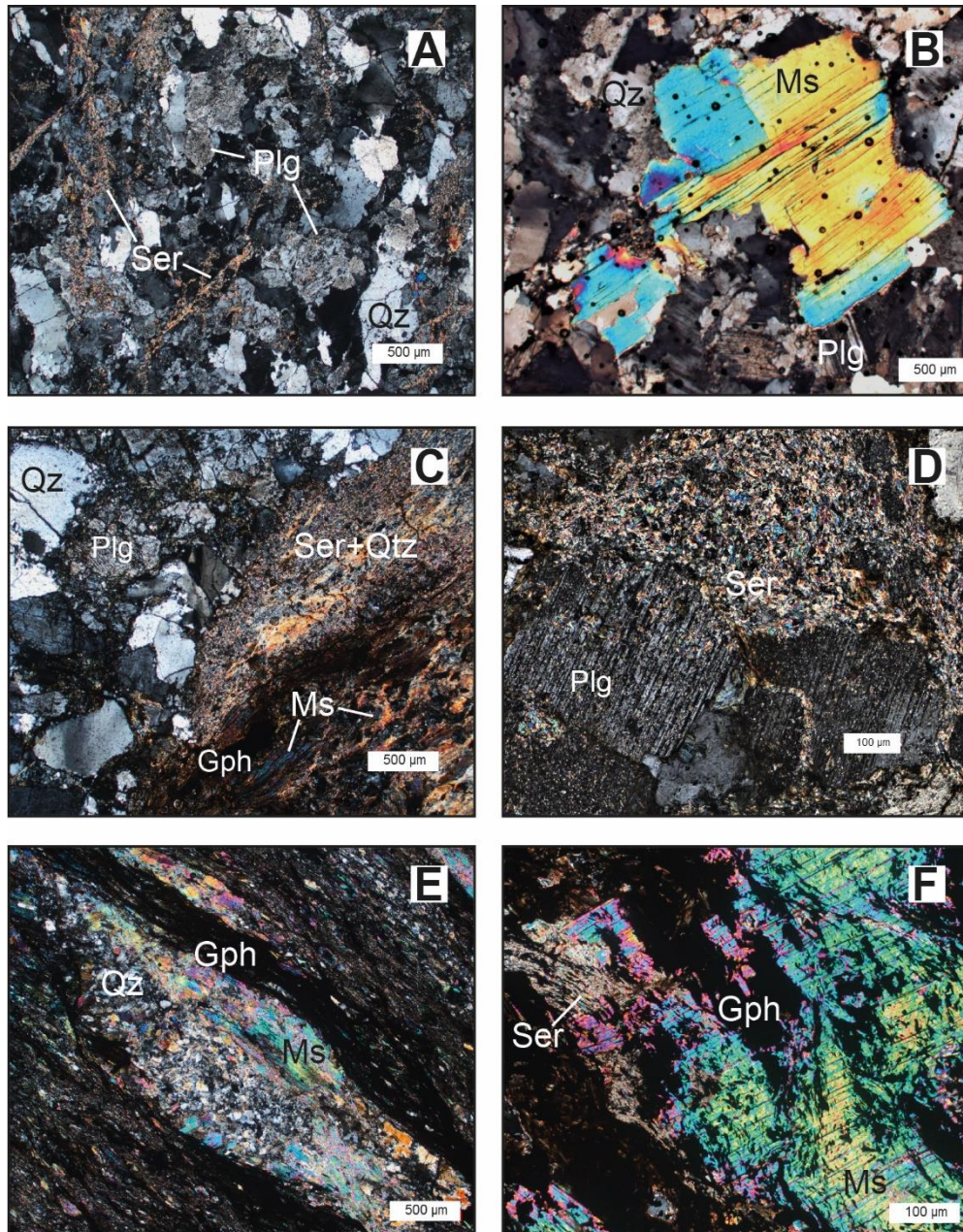
Figure 6. Transmitted-light photomicrographs of host rocks from the deposits, showing different degrees of hydrothermal alteration. Samples are from the Novo Horizonte (A, B), Morro dos Borges (C, D and F), and Tucano (E) deposits. A. Muscovite monzogranite, with feldspar crystals partially replaced by sericite B. Large magmatic muscovite crystal. C. Interface between partially altered granite microlithon and mylonitic groundmass composed of fine quartz+sericite and coarser intergrown graphite and muscovite lamellae. D. Detail of plagioclase crystal with partial sericite alteration. E. Graphite-biotite-muscovite schist displaying a domain with quartz and muscovite enveloped by graphite lamellae. F. Graphite-muscovite schist sample from the contact zone in Fig. 5B, showing coarse-grained muscovite with graphite inclusions. Qz: quartz; Ms: muscovite; Ser: sericite; Plg: plagioclase; Gph: graphite.

3.3. Hydrothermal alteration and gold mineralization

Hydrothermal alteration is characterized by leaching of the granitic wall rock, forming an alteration assemblage consisting of muscovite + quartz ± chlorite ± biotite. Pervasive alteration is limited to centimeter-wide zones, up to a few tens of centimeters, surrounding mineralizations. The hydrothermal alteration related to the ore itself is characterized by strong silicification, with varying amounts of sulfide and a muscovite ± chlorite proximal alteration paragenesis. Muscovite in these zones has a dark color, with a blueish to greenish tint. Very fine-grained sericitic groundmass constitute millimeter to centimeter-thick anastomosing layers in the mylonite (Fig. 7A-D). Distal alteration is restricted to a zone of a few tens of meters away from the shear zone within the granite, consisting of weak sericite and chlorite alteration. Hydrothermal chlorite occurs as a minor to trace phase both within and near the mineralized muscovite-quartz mylonite, developing also a centimeter-thick halo containing abundant <0.01 mm lamellae surrounding late mineralized quartz veins (Fig. 7F), and replacing biotite as a product of more distal alteration. Graphite, while not a hydrothermal mineral itself in this context, often occurs accompanying hydrothermal minerals in the contact zone, sometimes including gold-associated sulfides.
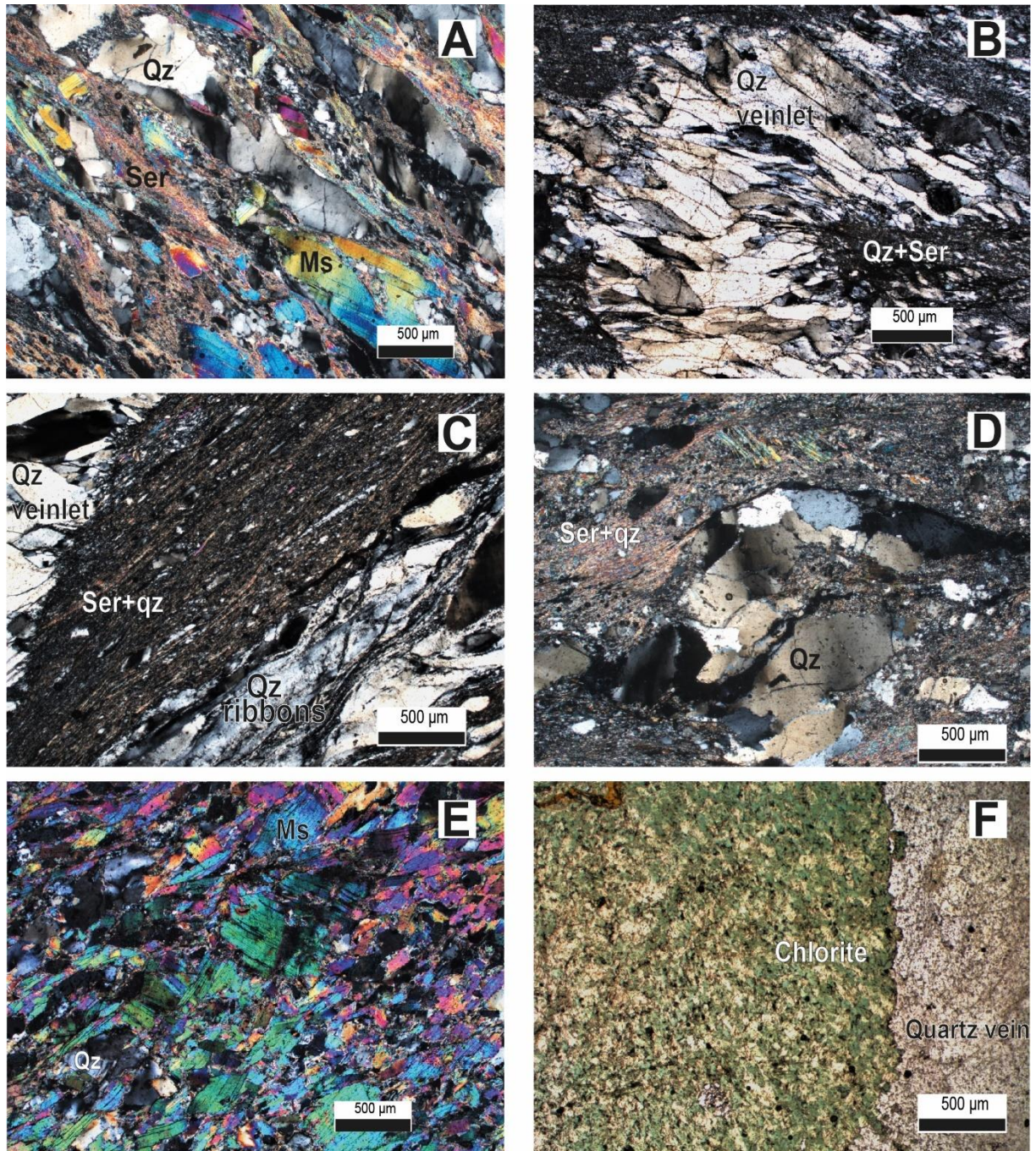
Figure 7. Photomicrographs of mylonite samples in the contact zone from Morro dos Borges (A-D) and Novo Horizonte (E, F). A: Muscovite-quartz mylonite with milimeter-thick quartz ribbons and relict primary muscovite grain. B: Silicified mylonite containing sheared quartz veinlets cross-cutting the foliation. C: Muscovite-quartz mylonite with quartz ribbons and a cross-cutting quartz veinlet. D: Sigmoidal quartz porphyroblast, with strongly recrystallized quartz displaying lobate interfingering grain boundaries and undulose extinction. E and F: Samples of the altered wallrock adjacent to mineralized veins, with massive aggregates of coarse muscovite (E) and fine-grained chlorite lamellae (F). Qz: quartz; Ms: muscovite; Ser: sericite.

Gold mineralization is associated with quartz veins, sulfides, and muscovite in muscovite-quartz mylonite, with some differences observed between the deposits, and even within a single deposit. The main form of occurrence is associated with muscovite and ore minerals in milimeter to submilimiter-thick microfractures in quartz. Host quartz constitutes veins of varying thickness, as well as pinched-out quartz pockets containing thin muscovite sheets. These quartz veins, veinlets and segregations that are parallel to either C or S foliations, compose either a strongly silicified mineralized segment, or an individual thick vein within the mylonite, a few tens of centimeters to 1-2 meters thick. The quartz associated with the mineralized veins is either smoky or milky in aspect, and gold grains are concentrated in the sulfide and muscovite-rich zones. Quartz veins display various states of deformation. Multiple stage veining with re-shearing and separation surfaces are common (Figs. 7B and 8A), with significant variation between recrystallization textures and grain sizes of individual quartz crystals. These veins occasionaly contain platy aggregates of fine-grained graphite and muscovite lamellae, occurring either along vein walls or filling fractures associated with sulfides. Free gold grains range between 0.01 and 0.2 mm in size, and appear either closely associated with sulfides or in contact with gangue minerals. Gold grains associated with gangue are frequently enclosed in deformed muscovite grains elongated parallel to foliation, preferentially in the margins of these grains. A magmatic origin has been suggested for such deformed muscovite in muscovite-quartz mylonite due to its high Ti contents, with rims showing lower Ti and, therefore, a hydrothermal character for the re-equilibrated border of these grains (Cunha, 2006; Menez, 2014). Finer-grained muscovite has TiO_2 lower than 0.6 wt. %, which allows to designate a secondary character for the mineral according to the criteria of Miller et al. (1981).

Overall, sulfide contents among deposits are low, in the order of 1% for Novo Horizonte samples with disseminated sulfides, and only trace amounts of very fine-grained pyrite in Morro dos Borges, and <0.1 mm arsenopyrite grains in mineralized veins from the Tucano deposit. In mineralized muscovite-quartz mylonite samples from Novo Horizonte, gold occurs along with arsenopyrite and pyrite, with the former being more abundant (Figs. 9C and D). Lower gold contents are found in disseminated form associated with 0.1-0.4 mm sulfide grains in fine-grained chlorite-muscovite layers in schist immediately adjacent to the contact zone. Arsenopyrite is the main sulfide phase associated with gold at Novo Horizonte, occurring as 0.1-0.5

mm crystals (Fig. 9B-F), both disseminated and in quartz veins. In disseminated form, euhedral to subhedral grains of arsenopyrite occurr along the foliation and exhibit in some cases skeletal textures with gangue inclusions, while preserving external euhedral rims (Fig. 9D). Both in sulfide aggregates within quartz veins and at the contact between vein and wallrock, gold occurs in intimate spacial relationship with different sulfide phases, as, for example, < 0.05 mm inclusions in the latter (Figs. 9E and F). Sulfide minerals in veins at Novo Horizonte occur in the following order of decreasing abundance: arsenopyrite, chalcopyrite, pyrite, galena (Fig. 9G), sphalerite (Fig. 9H), and pyrrhotite. Pyrrhotite appears as <0.1 mm inclusions in arsenopyrite. In the oxidized zone, malachite, chalcocite and covellite were formed from chalcopyrite (Figs. 9A, G and H), and hematite also occurs. A crystallization order beginning with pyrrhotite, followed by arsenopyrite, chalcopyrite, galena, sphalerite and pyrite was determined petrographically for the Novo Horizonte mineralized veins (Table 2). In contrast, at the Aurumina deposit gold is associated with quartz veins containing centimeter-scale pockets of coarse-grained pyrite, arsenopyrite, chalcopyrite, galena and sphalerite. At Buraco do Ouro, chalcopyrite and pyrite only occur as trace amounts , and gold is related to Bi-, As- and PGE-bearing selenides, sperrylite and uraninite. Paragenetic associations, mineralization style and structural controls of the deposits are summarized in Table 1.

	Novo Horizonte	Morro dos Borges	Tucano	Aurumina	Buraco do Ouro
Mineralization style	Disseminated in muscovite-quartz mylonite and in quartz veins	Disseminated in muscovite-quartz mylonite	Quartz veins	Quartz-carbonate vein	Disseminated in muscovite-quartz mylonite
Structural control	Silicified orebodies along the "S" foliation and veins parallel to the "C" foliation	Silicified orebodies along the "S" foliation	Veins parallel to the "C" foliation	Vein parallel to the "C" foliation	Silicified orebodies along the "S" foliation
Ore paragenesis	Arsenopyrite (disseminated) and arsenopyrite-pyrrhotite-pyrite-chalcopyrite-galena-sphalerite in veins	Pyrite	Arsenopyrite	Arsenopyrite-pyrrhotite-pyrite-chalcopyrite-galena-sphalerite-greenockite	Guanajuatite, kalungaite, mertieite I and II, sperrylite, padmaite, bohdanowiczite, clausthalite, uraninite, and Ag-Pb-Bi-Se minerals

Table 1. Comparison between the characteristics of the deposits studied in this work and the deposits of Aurumina (Cunha, 2006) and Buraco do Ouro (Menez and Botelho, 2017).
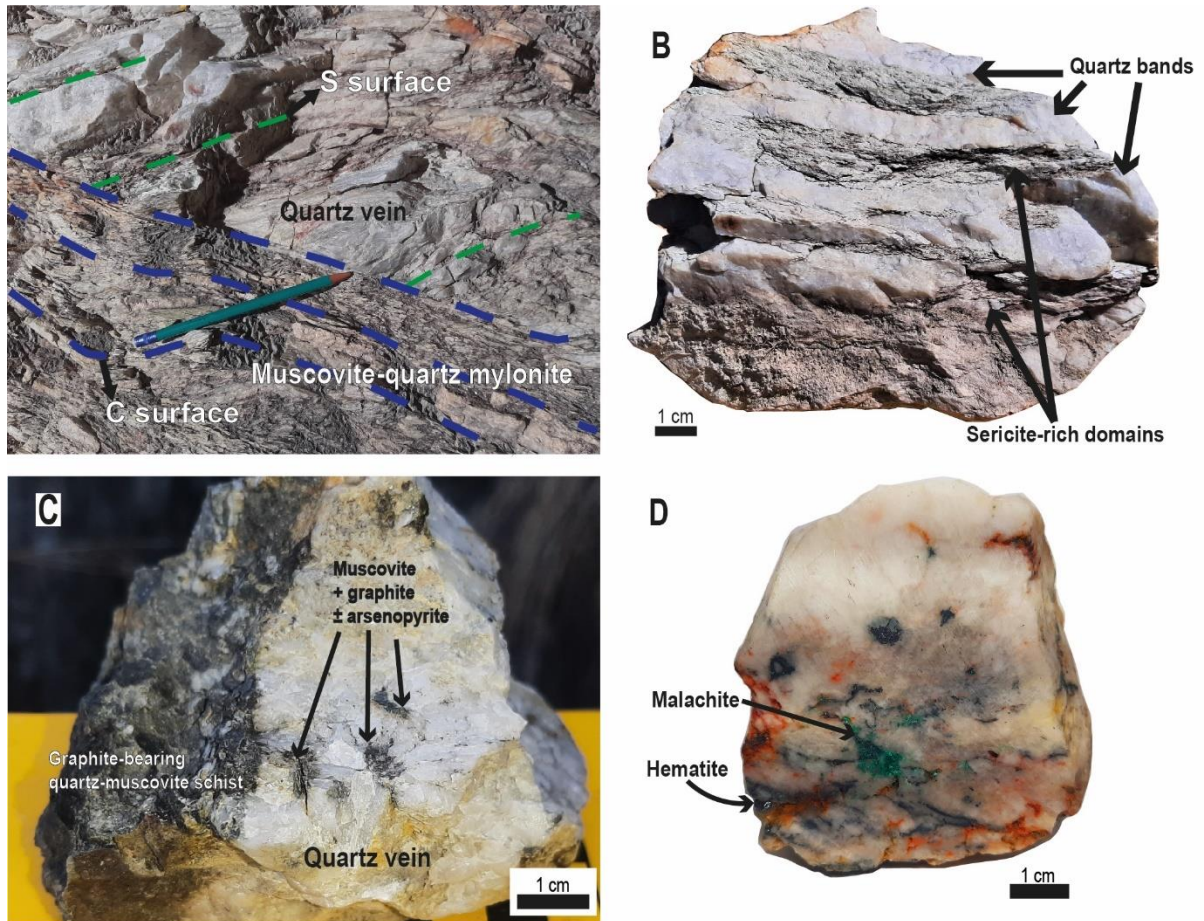
Figure 8. A. Mylonite and barren quartz vein outcrop in the Morro dos Borges deposit, with S foliation surface imprinted in the vein. B. Sample of muscovite-quartz mylonite, formed as a sheared, silicified alteration product of biotite-muscovite granite, with quartz and sericite-rich domains indicated. C. Quartz vein from the Tucano deposit showing the contact between schist and very fine-grained muscovite+graphite±arsenopyrite aggregates both filling fractures and as inclusions. D. Mineralized quartz vein sample from Novo Horizonte with malachite and hematite.
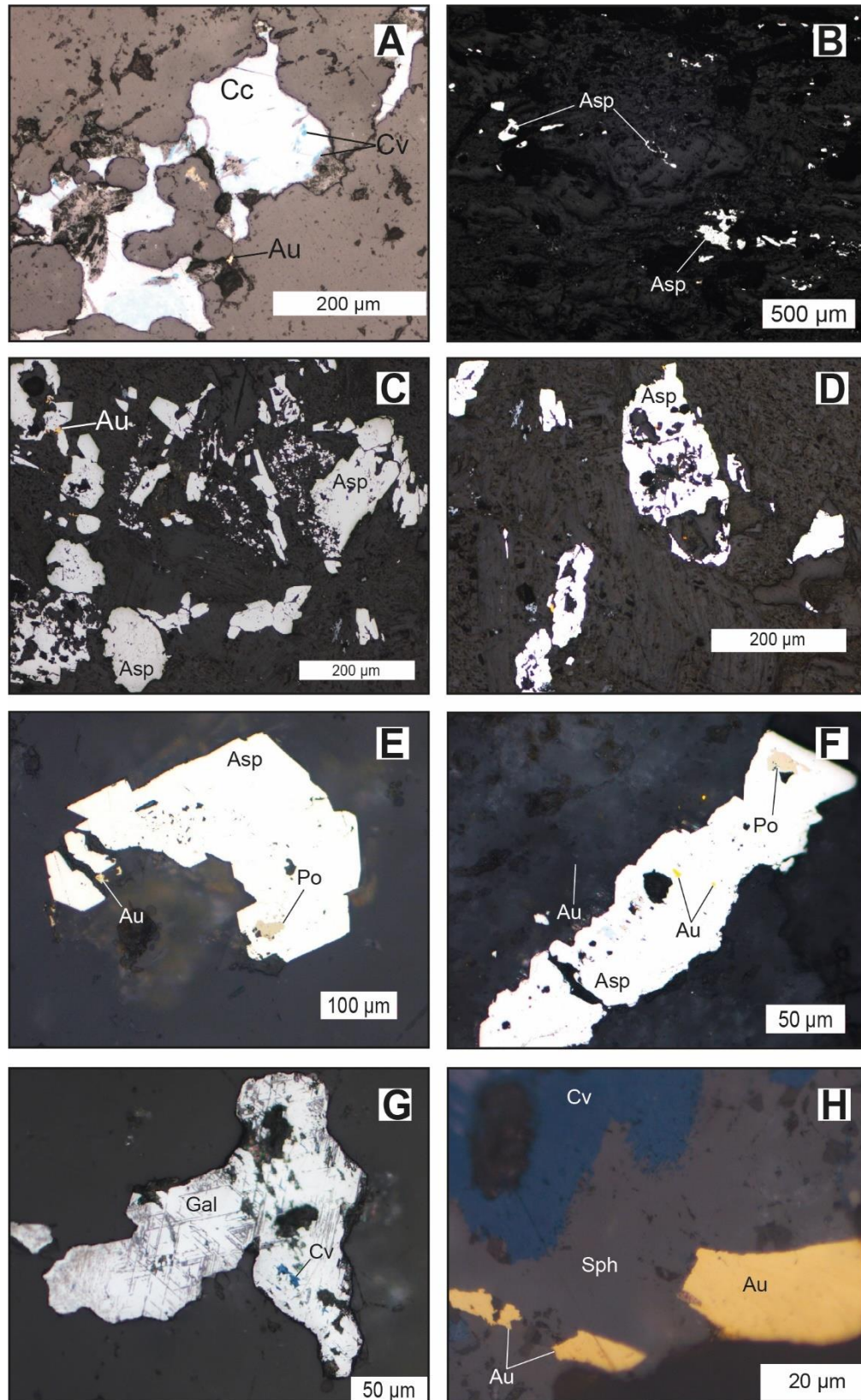
Figure 9. Reflected light photomicrographs of ore samples from the Novo Horizonte deposit. A. Chalcocite and covellite associated with gold in quartz vein. B. Fine-grained arsenopyrite crystals disseminated along foliation in muscovite-quartz mylonite. C. Arsenopyrite crystals in muscovite-quartz mylonite. D. Disseminated arsenopyrite with gangue inclusions. E. Subhedral arsenopyrite crystal with pyrrhotite

inclusion and adjacent gold grain. F. Subhedral arsenopyrite crystal containing pyrrhotite and gold inclusions. G. Galena and covellite association in quartz vein. H. Sphalerite, covellite and gold grains in quartz vein. Cc: chalcocite; Cv: covellite; Au: gold; Asp: arsenopyrite; Po: pyrrhotite; Gal: galena; Sph: sphalerite.

4. Analytical methods

The mineralogical composition of mineralized zones and host rocks was studied using both transmitted- and reflected-light microscopy at the University of Brasília. Whole-rock chemical analyses were performed by ACME Laboratories in Canada using combined ICP-ES and ICP-MS, with multi acid digestion after lithium borate fusion for major and trace elements. Acqua regia extraction was used for base metals, while Au was analized by fire assay. Major element oxides determined, with results expressed as wt. %, were SiO_2, TiO_2, Al_2O_3, Fe_2O_3, MnO Cr_2O_3, MgO, CaO, Na_2O, K_2O, and P_2O_5. Leco technique was used for total S and C. Trace elements determined were Be, Cs, Rb, Ba, Sr, Ga, Ni, Co, Cu, Pb, Zn, Ni, Mo, Au, Ag, As, Cd, Sb, Bi, Se, Tl, Hg, Th, U, Zr, Hf, Sn, Nb, Ta, W, V, Sc and REES. Pt, Pd and Rh were also analyzed in some samples at ActLabs, with lectures made by Instrumental Neutron Activation Analysis (INAA) and ICP-MS, respectively, after fire assay fusion. In total, 31 samples were analyzed for whole-rock geochemistry, and 7 samples were selected for PGE analysis.

For EPMA, a JEOL JXA-8230 microanalyzer with five coupled wavelength-dispersive spectrometers (WDS) was used. The analytical conditions consisted of an accelerating voltage of 20 kV and a beam current of 20 nA. 18 spot analysis were performed on arsenopyrite grains and 12 on chalcocite grains, of a mineralized muscovite-quartz mylonite sample (for arsenopyrite) and of a mineralized quartz vein sample (for arsenopyrite and chalcocite) from the Novo Horizonte deposit. Sulfur isotope analyses of 10 selected arsenopyrite grains and of 8 pyrite grains were carried out on a mineralized quartz vein sample from the Novo Horizonte deposit, at the Geochronology Laboratory of the University of Brasília using a Multicollector LA-ICP-MS Thermo-Finnigan Neptune coupled to a Nd-YAG 213 nm NewWave laser. Sulfide grains of mineralized quartz vein samples from the Aurumina mine (sphalerite, pyrrhotite and pyrite) were prepared through dissolved sulfide collection with cadmium acetate and the sulfur isotopic compositions were determined using a

Finnigan MAT 251 mass spectrometer at an ion acceleration voltage of 10 kV at the Isotope Science Lab, University of Calgary, Canada.

5. Analytical results

5.1. Whole-rock chemical analysis

Data obtained for major and trace element compositions of whole-rock chemical analysis are listed in Table 1. Data for Au, Pt, Pd and Rh of selected biotite-muscovite granite, schist and quartz vein samples are listed on Table 2. Major element binary plots for schist and granitic rocks in Figures 10 and 11, respectively, show variations of TiO_2, Al_2O_3, Fe_2O_3, MgO, K_2O, Na_2O, and CaO with SiO_2. Data from the Aurumina deposit from Cunha (2006), Aurumina Suite granite samples from Cuadros et al. (2017a) and Ticunzal Formation schist samples from Cuadros et al. (2017b) were also plotted for comparison. In the case of the data from Cuadros et al. (2017a; 2017b), samples are unrelated to any deposit, shown to represent regional values for the respective units.

Sample	Rock Type	Location	SiO2	TiO2	Al2O3	Fe2O3	MnO	Cr2O3	MgO	CaO	Na2O	K2O	P2O5
NH4-VI-A	Schist	Novo Horizonte	68.93	1.13	12.97	5.82	0.09	0.014	4.24	0.02	0.04	3.19	0.03
NH4-VII-A	Schist	Novo Horizonte	52.21	1.24	18.40	9.98	0.03	0.007	6.67	<0.01	0.06	5.11	0.02
NH-6-B1	Schist	Novo Horizonte	44.05	0.88	26.65	6.63	0.04	0.023	2.23	0.26	0.17	8.45	0.05
NH-13	Schist	Novo Horizonte	65.48	0.99	17.62	3.89	0.03	0.002	1.06	0.29	0.14	6.90	0.30
NH-15	Schist	Novo Horizonte	59.57	0.50	18.04	9.13	0.09	0.017	1.48	0.07	0.05	5.14	0.24
NH-16-A	Schist	Novo Horizonte	60.61	0.63	18.22	8.66	0.04	0.014	0.98	0.01	0.06	5.39	0.09
NH-17	Schist	Novo Horizonte	62.40	0.64	18.20	7.14	0.03	0.013	0.99	0.02	0.08	4.83	0.13
TU-15	Schist	Tucano	60.54	0.65	19.32	6.09	0.04	0.013	2.04	0.15	0.37	4.47	0.08
TU-16	Schist	Tucano	66.51	0.49	15.61	5.68	0.05	0.017	1.70	0.14	0.17	3.73	0.06
TU-17	Schist	Tucano	83.20	0.22	9.88	0.72	<0.01	0.021	0.62	0.03	0.04	3.41	<0.01
TU-20	Schist	Tucano	87.97	0.05	4.34	4.51	0.17	0.025	0.12	0.02	0.04	0.95	0.07
TU-20-A	Schist	Tucano	77.72	0.31	9.00	6.84	0.01	0.299	0.33	0.01	0.12	2.66	0.08
TU-20-B	Schist	Tucano	74.09	0.50	12.88	4.94	<0.01	0.017	0.41	<0.01	0.18	3.70	0.03
NE-3	Schist	Morro dos Borges	67.75	0.34	14.29	3.10	0.02	0.011	1.10	<0.01	0.04	4.83	0.06
TF-09-33	Schist	Regional	64.37	1.14	18.14	4.44	0.03	0.015	0.82	0.02	0.25	5.15	0.02
NH-7-B	Granite	Novo Horizonte	76.25	0.06	12.59	1.13	<0.01	<0.002	0.10	0.35	3.00	4.93	0.22
NH-14	Granite	Novo Horizonte	71.35	0.04	16.20	0.50	<0.01	<0.002	0.15	0.59	3.61	5.61	0.24
NU-I	Granite	Novo Horizonte	70.57	<0.01	16.88	0.19	0.02	<0.002	0.11	0.06	5.53	4.24	0.14
NU-II	Granite	Novo Horizonte	70.14	<0.01	16.93	0.30	0.03	<0.002	0.12	0.19	4.18	6.72	0.23
NH-10	Muscovite-quartz mylonite	Novo Horizonte	69.48	0.26	14.57	4.42	<0.01	<0.002	1.66	<0.01	0.05	6.31	0.04
NH-11	Muscovite-quartz mylonite	Novo Horizonte	72.54	0.63	12.20	6.38	<0.01	0.007	0.76	0.02	0.05	3.84	0.25
NH-12-A	Muscovite-quartz mylonite	Novo Horizonte	64.63	0.75	17.86	4.42	0.02	0.008	1.53	0.04	0.05	7.06	0.12
NE-4	Muscovite-quartz mylonite	Morro dos Borges	72.01	0.08	15.53	1.40	<0.01	<0.002	0.94	0.01	0.12	7.26	0.03
NE-1-A	Silicified mylonite	Morro dos Borges	88.13	0.11	6.00	1.38	<0.01	0.011	0.40	<0.01	0.02	2.31	0.02
NE-1-B1	Silicified mylonite	Morro dos Borges	87.08	0.18	6.90	0.78	<0.01	0.101	0.54	<0.01	0.03	2.62	<0.01
NE-1-B2	Silicified mylonite	Morro dos Borges	87.11	0.18	6.61	1.01	<0.01	0.223	0.67	<0.01	0.02	2.44	0.01
NE-1-C	Silicified mylonite	Morro dos Borges	86.43	0.03	7.59	0.82	<0.01	0.009	0.71	<0.01	0.03	2.97	<0.01
NE-2	Silicified mylonite	Morro dos Borges	87.18	0.26	5.73	1.56	0.01	0.140	0.74	0.03	0.02	2.21	0.03
NH4-V-A	Quartz Vein	Novo Horizonte	97.18	<0.01	0.14	1.55	<0.01	0.002	0.01	<0.01	<0.01	0.02	<0.01
NH4-V-B	Quartz Vein	Novo Horizonte	97.16	<0.01	0.88	0.50	0.01	0.002	0.89	<0.01	<0.01	0.03	<0.01
NH4-VII-B	Quartz Vein	Novo Horizonte	99.18	<0.01	0.08	<0.04	0.01	<0.002	<0.01	<0.01	<0.01	0.02	0.02

LOI	Sum	TOT/C	TOT/S	Be	Cs	Rb	Ba	Sr	Ga	Co	Cu	Pb	Zn	Ni	Mo	Au	Ag
3.2	99.70	<0.02	<0.02	2	5.5	166.9	931	20.6	23.9	31.8	175.1	17.8	139	32.8	<0.1	1.9	0.2
5.9	99.69	0.02	<0.02	6	7.0	209.4	538	6.8	24.2	23.4	4.7	4.2	188	49.2	<0.1	<0.5	<0.1
10.3	99.75	5.56	0.02	6	14.7	438.7	865	39.7	38.7	15.8	13.7	6.9	62	42.4	2.0	89.9	<0.1
3.0	99.72	0.02	<0.02	6	17.9	419.0	421	31.0	29.2	5.2	3.9	34.4	27	2.2	<0.1	1.2	<0.1
5.3	99.59	0.04	<0.02	5	12.2	314.5	854	40.1	24.4	21.8	772.9	11.6	117	42.9	<0.1	1.4	<0.1
5.2	99.85	0.25	<0.02	5	13.3	325.9	687	10.4	25.5	6.8	25.0	16.5	28	15.3	<0.1	<0.5	<0.1
5.4	99.86	0.69	<0.02	7	11.9	285.9	548	22.9	22.7	12.5	42.1	6.8	45	55.5	0.4	0.7	<0.1
6.0	99.76	0.58	<0.02	8	115.1	335.5	803	49.9	27.5	9.0	13.4	5.1	188	45.3	<0.1	1.5	0.2
5.7	99.83	1.06	<0.02	7	65.9	268.3	623	39.1	26.3	16.2	16.5	6.2	175	42.2	<0.1	2.5	0.3
1.8	99.94	0.03	<0.02	5	34.8	228.3	230	6.0	20.1	1.9	1.8	3.2	6	1.9	<0.1	1.7	0.4
1.6	99.91	0.05	<0.02	18	9.8	74.7	375	24.4	8.4	13.1	99.8	138.6	34	13.1	0.8	101.4	2.5
2.5	99.85	0.17	<0.02	6	26.0	199.7	321	15.5	15.4	4.2	27.6	201.6	29	7.7	1.6	21.6	0.3
3.1	99.86	0.54	<0.02	3	27.0	235.0	502	18.4	19.3	2.2	18.8	25.8	7	3.8	0.5	4.2	<0.1
8.3	99.86	5.65	<0.02	8	17.0	296.3	291	8.9	22.8	1.9	78.0	14.9	19	9.1	<0.1	1.5	<0.1
5.5	99.86	1.82	<0.02	3	7.1	194.3	578	20.1	22.5	6.6	17.4	4.2	14	7.2	0.3	0.6	<0.1
1.1	99.71	<0.02	<0.02	2	5.9	158.7	683	84.1	16.5	n. a.	5.4	5.9	5	1.6	0.4	2.3	<0.1
1.7	99.95	0.03	<0.02	3	3.2	197.7	309	122.0	18.4	0.6	0.9	11.2	2	0.2	<0.1	<0.5	<0.1
2.2	99.95	0.05	<0.02	2	1.8	120.9	343	77.5	7.9	0.7	1.2	6.0	5	0.6	<0.1	<0.5	<0.1
1.1	99.93	0.03	<0.02	2	13.7	204.9	438	110.0	10.5	0.6	1.0	13.9	3	0.3	<0.1	<0.5	<0.1
2.9	99.74	<0.02	<0.02	4	7.1	232.9	651	5.3	22.5	2.1	1.9	2.9	2	0.3	0.1	<0.5	<0.1
3.0	99.69	0.05	<0.02	5	9.0	247.9	897	46.8	26.0	5.8	38.2	4.5	12	5.8	<0.1	3.0	<0.1
3.3	99.78	0.06	<0.02	3	14.8	348.5	486	11.1	24.1	8.4	17.2	27.3	36	8.0	<0.1	1.6	<0.1
2.4	99.77	<0.02	<0.02	5	14.9	363.1	516	24.6	22.9	n. a.	2.9	6.8	5	1.0	0.2	4.6	<0.1
1.5	99.87	<0.02	<0.02	3	6.7	146.3	258	5.8	11.6	n. a.	3.5	6.0	3	1.8	0.1	8.7	<0.1
1.7	99.90	0.35	<0.02	3	9.1	165.8	218	6.6	15.6	1.4	4.7	11.2	5	2.5	<0.1	6017.5	0.6
1.6	99.90	0.06	<0.02	4	12.6	165.1	247	5.5	15.8	2.2	6.3	3.8	9	6.6	<0.1	249.4	0.1
1.3	99.93	0.02	<0.02	3	10.3	179.0	154	5.7	15.2	1.8	6.7	2.5	9	2.7	<0.1	251.7	0.2
1.7	99.62	0.19	<0.02	4	15.9	182.4	195	6.4	11.8	n. a.	27.1	4.8	25	9.6	0.5	101.6	<0.1
0.6	99.47	0.03	0.07	<1	<0.1	1.0	70	1.8	0.8	0.3	4170.1	0.7	1	0.4	0.3	3392.4	12.4
0.6	100.03	0.03	<0.02	<1	<0.1	1.2	4	1.7	2.1	12.0	21.1	0.6	30	10.0	<0.1	<0.5	0.4
0.8	100.03	<0.02	<0.02	<1	<0.1	0.9	10	1.3	<0.5	4.2	1.1	1.7	2	1.3	<0.1	<0.5	<0.1

Sc	V	W	Ta	Nb	Sn	Hf	Zr	U	Th	Hg	Tl	Se	Bi	Sb	Cd	As
23	266	5.2	1.0	14.1	2	6.6	207.6	5.3	10.9	<0.01	<0.1	<0.5	0.3	<0.1	<0.1	4.2
29	189	2.0	1.0	14.8	2	8.1	264.3	2.8	12.1	<0.01	<0.1	<0.5	0.1	<0.1	<0.1	3.9
25	144	7.4	1.2	14.9	4	7.9	241.7	7.1	22.4	<0.01	<0.1	<0.5	1.6	<0.1	<0.1	603.9
4	23	8.8	0.8	18.3	19	17.0	532.2	14.3	186.4	<0.01	0.6	<0.5	1.9	<0.1	<0.1	2.9
17	113	1.6	0.7	9.4	4	5.0	186.8	6.5	17.3	<0.01	0.2	1.2	2.8	<0.1	<0.1	1.9
18	126	3.0	0.7	13.0	1	5.7	180.6	7.4	19.7	<0.01	0.1	<0.5	0.1	<0.1	<0.1	1.3
19	113	2.2	0.8	12.3	2	5.2	172.4	7.0	17.1	<0.01	<0.1	0.5	0.5	<0.1	<0.1	28.4
19	120	6.9	1.0	13.2	58	5.0	171.6	8.4	16.7	<0.01	0.4	0.5	0.1	<0.1	<0.1	4.2
16	109	3.5	0.8	11.8	13	4.6	144.7	6.8	14.5	<0.01	0.3	<0.5	3.2	<0.1	<0.1	7.8
5	50	1.6	3.3	10.4	34	3.2	138.5	4.1	6.9	<0.01	0.2	<0.5	1.4	<0.1	<0.1	1.8
3	38	4.9	0.2	2.7	6	0.9	37.5	8.7	2.3	0.06	0.3	4.8	52.9	0.3	<0.1	77.6
8	84	3.1	0.4	5.2	4	3.1	101.7	6.0	5.3	<0.01	0.1	1.0	146.7	0.1	<0.1	32.4
13	119	3.1	0.5	7.5	3	4.2	145.3	7.3	6.6	<0.01	<0.1	0.7	0.9	<0.1	<0.1	15.1
8	96	1.1	0.6	7.1	3	3.7	122.5	7.7	9.1	<0.01	0.2	<0.5	0.9	<0.1	<0.1	3.3
16	85	5.8	1.9	20.3	5	7.7	242.9	2.5	20.4	<0.01	0.1	<0.5	1.5	<0.1	<0.1	<0.5
2	9	n. a.	3.2	7.8	7	2.1	44.8	1.0	4.4	<0.01	<0.1	<0.5	<0.1	<0.1	<0.1	11.9
1	<8	<0.5	0.2	3.4	3	2.4	59.9	3.6	4.4	<0.01	<0.1	<0.5	1.4	<0.1	<0.1	0.7
1	<8	0.6	0.3	2.6	2	1.3	35.0	2.0	3.3	<0.01	<0.1	<0.5	0.3	<0.1	<0.1	1.0
1	<8	2.1	0.8	3.9	9	0.9	23.0	1.7	1.1	<0.01	<0.1	<0.5	1.4	<0.1	<0.1	1.4
11	110	1.0	3.2	51.6	8	14.8	468.3	4.2	49.4	<0.01	<0.1	<0.5	<0.1	<0.1	<0.1	3.3
17	121	1.8	1.1	15.5	3	6.0	214.8	1.6	19.9	<0.01	<0.1	1.1	<0.1	<0.1	<0.1	4.6
8	50	2.0	0.9	12.6	2	10.2	313.1	10.0	74.1	<0.01	0.2	<0.5	1.3	<0.1	<0.1	1.0
3	17	n. a.	2.8	12.9	13	1.4	38.0	1.4	2.1	<0.01	0.2	<0.5	1.7	<0.1	<0.1	0.7
2	22	n. a.	1.0	4.9	3	1.2	41.4	1.0	2.0	<0.01	0.1	<0.5	5.3	<0.1	<0.1	0.7
4	47	1.3	0.7	5.9	4	1.7	62.0	1.5	3.9	0.01	0.2	<0.5	4.8	<0.1	<0.1	1.1
4	49	1.4	0.4	5.1	4	1.7	58.9	1.7	4.4	<0.01	0.2	<0.5	2.7	<0.1	<0.1	0.7
1	38	0.9	0.4	2.2	4	0.3	16.3	1.4	1.1	<0.01	0.3	<0.5	1.8	<0.1	<0.1	0.7
4	58	n. a.	3.0	7.6	2	4.2	180.2	3.3	6.7	<0.01	0.5	<0.5	2.2	<0.1	<0.1	2.5
<1	26	2.2	<0.1	0.5	<1	<0.1	1.4	<0.1	<0.2	<0.01	<0.1	5.2	5.7	<0.1	<0.1	0.6
<1	14	<0.5	<0.1	<0.1	<1	<0.1	0.7	<0.1	<0.2	<0.01	<0.1	<0.5	<0.1	<0.1	<0.1	1.2
<1	<8	<0.5	<0.1	0.2	<1	<0.1	1.4	<0.1	<0.2	<0.01	<0.1	<0.5	<0.1	<0.1	<0.1	0.6

Y	La	Ce	Pr	Nd	Sm	Eu	Gd	Tb	Dy	Ho	Er	Tm	Yb	Lu
39.0	45.9	85.7	11.37	41.9	8.20	1.71	7.07	1.18	6.89	1.29	3.99	0.62	3.58	0.57
55.8	68.1	104.0	16.40	60.0	11.44	2.29	10.35	1.76	9.85	1.86	5.26	0.79	4.59	0.71
35.4	66.7	143.4	15.53	53.4	9.45	1.85	7.39	1.18	6.64	1.18	3.65	0.59	3.82	0.62
14.5	150.7	436.2	50.11	184.3	27.32	1.65	11.98	1.12	3.37	0.34	0.71	0.10	0.73	0.09
50.9	210.1	402.3	55.52	199.3	30.92	4.82	19.23	2.79	12.25	2.02	5.44	0.78	4.76	0.62
11.4	4.4	21.2	1.22	4.8	1.06	0.25	1.14	0.27	1.69	0.44	1.59	0.29	1.93	0.30
14.4	11.5	20.7	2.23	8.2	1.72	0.30	1.70	0.34	2.00	0.47	1.53	0.26	1.92	0.29
34.2	48.8	107.4	11.60	41.9	7.86	1.44	6.57	1.12	6.03	1.32	3.64	0.57	3.47	0.49
21.8	38.1	79.1	8.76	35.0	6.00	1.07	4.88	0.74	4.05	0.76	2.33	0.37	2.31	0.35
7.2	17.8	35.5	3.77	13.4	2.62	0.51	1.95	0.28	1.33	0.25	0.82	0.14	0.92	0.15
8.5	31.5	48.1	6.63	25.3	4.91	1.04	3.78	0.50	1.91	0.32	0.84	0.13	0.72	0.10
10.3	28.6	41.7	6.37	25.9	5.48	1.11	4.65	0.63	2.66	0.46	1.17	0.18	1.13	0.15
14.7	25.9	44.6	5.98	22.8	4.05	0.84	3.36	0.54	2.68	0.58	1.88	0.30	1.80	0.26
14.4	34.8	70.1	7.16	24.3	3.24	0.63	2.75	0.42	2.04	0.49	1.39	0.23	1.52	0.23
37.0	17.2	26.9	4.70	17.6	3.90	0.79	3.66	0.76	5.19	1.28	4.74	0.82	5.05	0.76
9.9	10.9	22.7	2.81	11.6	2.56	0.41	2.45	0.36	1.68	0.25	0.68	0.10	0.59	0.08
13.5	12.2	27.7	3.52	14.2	3.82	0.67	3.58	0.61	2.70	0.38	1.00	0.12	0.67	0.08
51.5	9.0	18.3	2.95	14.1	3.93	1.38	5.70	1.14	5.96	1.18	3.25	0.45	2.54	0.34
16.9	8.3	15.2	2.04	8.3	2.00	0.88	2.71	0.50	2.61	0.51	1.25	0.18	0.94	0.12
49.8	144.9	326.6	32.78	115.0	20.00	1.55	12.96	1.83	9.58	1.65	5.56	0.95	6.67	1.02
72.2	306.1	257.0	76.05	312.3	52.00	8.95	41.24	5.22	22.38	2.96	7.05	1.00	6.19	0.90
24.2	109.3	273.5	32.52	125.2	19.08	1.46	10.07	1.17	5.19	0.78	2.05	0.30	1.84	0.26
4.6	3.4	6.1	0.76	2.3	0.65	0.19	0.66	0.14	0.68	0.15	0.40	0.07	0.42	0.07
5.4	8.9	15.9	1.78	6.1	0.94	0.21	0.80	0.14	0.66	0.18	0.53	0.09	0.56	0.09
6.3	16.1	30.5	3.27	10.6	1.98	0.34	1.48	0.20	0.93	0.19	0.59	0.10	0.72	0.10
7.9	21.8	41.5	4.69	16.0	2.69	0.42	1.88	0.25	1.24	0.24	0.70	0.12	0.76	0.12
5.4	3.0	6.4	0.77	3.0	0.66	0.17	0.72	0.14	0.64	0.17	0.45	0.07	0.38	0.06
10.6	19.2	42.3	4.22	15.5	2.64	0.38	2.09	0.31	1.62	0.37	1.13	0.20	1.40	0.20
0.3	0.7	1.3	0.12	0.6	0.09	<0.02	0.05	0.01	0.05	<0.02	<0.03	<0.01	<0.05	<0.01
0.4	0.6	1.3	0.09	<0.3	0.08	<0.02	<0.05	0.02	0.07	<0.02	0.04	0.01	<0.05	<0.01
0.5	0.5	0.8	0.10	<0.3	0.09	0.02	0.07	0.01	0.07	0.02	0.06	0.01	0.07	0.01

Table 2. Whole-rock major (wt. %) and trace element (ppm, except for Au, expressed in ppb) data.

Granite samples have high SiO_2 (70.14-76.25 wt.%) and Al_2O_3 (12.59-16.93 wt.%) contents, Fe_2O_3 ranging from 0.19 to 1.13 wt.%, low MgO (average 0.12 wt.%) and CaO (0.19-0.59, average 0.30 wt.%), and K_2O and Na_2O of 4.24-6.72 wt.% and 3.53-5.53 wt.%, respectively. All granite samples have a strongly peraluminous signature, with Alumina Saturation Index values >1.1. Schist samples have much greater compositional variations, with SiO_2 ranging from 44.44 to 68.93 wt.%, Al_2O_3 from 12.97 to 26.65 wt.%, and K_2O varying from 3.19 to 8.45 wt.%. Fe_2O_3 and MgO contents are markedly higher in the schists than in the granites, with Fe_2O_3 ranging from 3.10 to 9.98 wt.%, and MgO up to 6.67 wt.%. Silicified schist samples with >70 wt.% SiO_2 are found at the contact zone in the Tucano deposit. All samples have low CaO contents (<1 wt. %). Differences in major element contents between granite and mylonite samples consist of lower Na_2O, CaO and P_2O_5 and relatively higher SiO_2, TiO_2, Fe_2O_3 and MgO, and, in the case of muscovite-rich mylonite samples, higher K_2O contents. K_2O values that are higher than average are found in samples rich in either fine- or coarse-grained muscovite aggregates. Average Fe_2O_3 contents are in general higher in mylonite than in granite samples (average of 2.5 wt.% in mylonite vs 0.5 wt.% in granite, with up to 6.38 wt.% in muscovite-rich mylonite). Granite samples analyzed in this work have compositions similar to those reported from the Aurumina deposit. Also, granite samples from the deposits and those reported by Cuadros et al. (2017a) have similar compositions for most major elements, with relatively lower proportions of TiO_2, Fe_2O_3, and MgO. Progressively higher SiO_2 values in mylonite and silicified schist samples reflect increasing degree of silicification, with replacement of feldspars and ferro-magnesian minerals by silica.

Schist samples at the contact zone, with pervasive mylonitic fabric and hydrothermal alteration, have Au contents of 100-200 ppb Au, indicating minor gold enrichment in wallrocks. Some of these samples also have high As contents, of up to 604 ppm, although several As-enriched samples display no anomalous Au contents. Some samples from the Tucano deposit also display Bi amounts of up to 146 ppm, highly anomalous when compared to other samples (1.6 ppm average Bi among all analyzed samples). Au concentrations obtained in silicified mylonite attain up to 6,017 ppb in Morro dos Borges, and up to 16,273 ppb in a quartz vein from Novo Horizonte. Biotite-muscovite granite samples from Novo Horizonte have up to 24.2 ppb Pd and 14.4 ppb Pt, while schist samples have up to 9.5 and 5.4 ppb Pd and Pt,

respectively, values that are similar to the ones obtained from a mineralized quartz vein sample (Table 2).

Sample	Rock Type	Au	Pt	Pd	Rh
NH2	Ticunzal schist (mineralization wallrock)	105	5.4	9.5	0.05
NH3	Ticunzal schist (mineralization wallrock)	191	2.5	2	0.05
NH5	Mineralized quartz vein	16273	5.4	8.1	0.49
99-VII-176	Biotite-muscovite granite	25	7	11.4	2.01
99-IV-56	Biotite-muscovite granite	32	0.6	5.2	0.73
99-IV-65	Biotite-muscovite granite	3	3.6	5.5	1.39
99-VII-139	Biotite-muscovite granite	38	14.4	24.2	2.49

Table 2. Au and PGE chemical analyses, in ppb, of selected samples from the Novo Horizonte deposit.
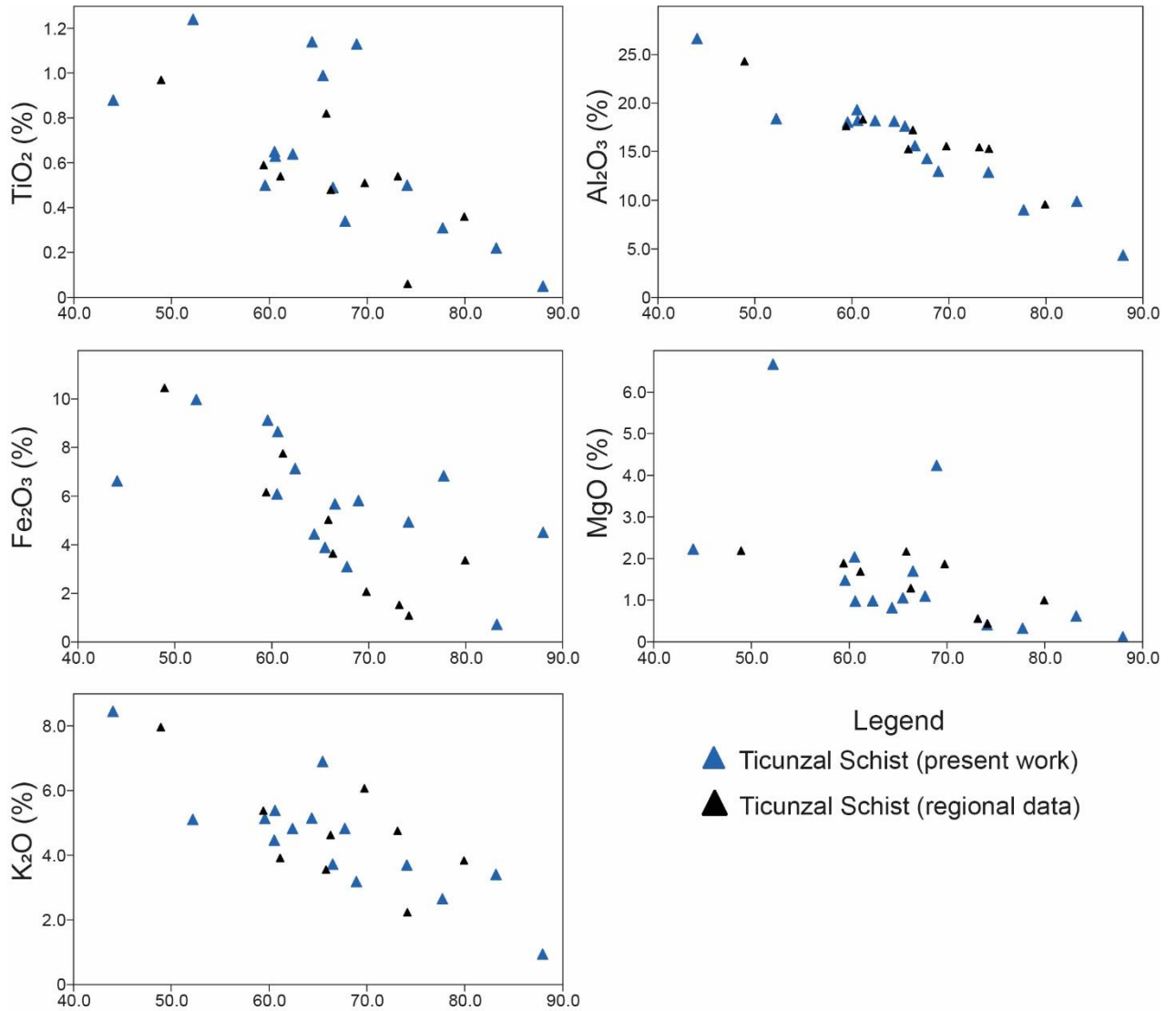
Figure 10. Harker diagrams of major-element oxides vs SiO$_2$ for schist samples.
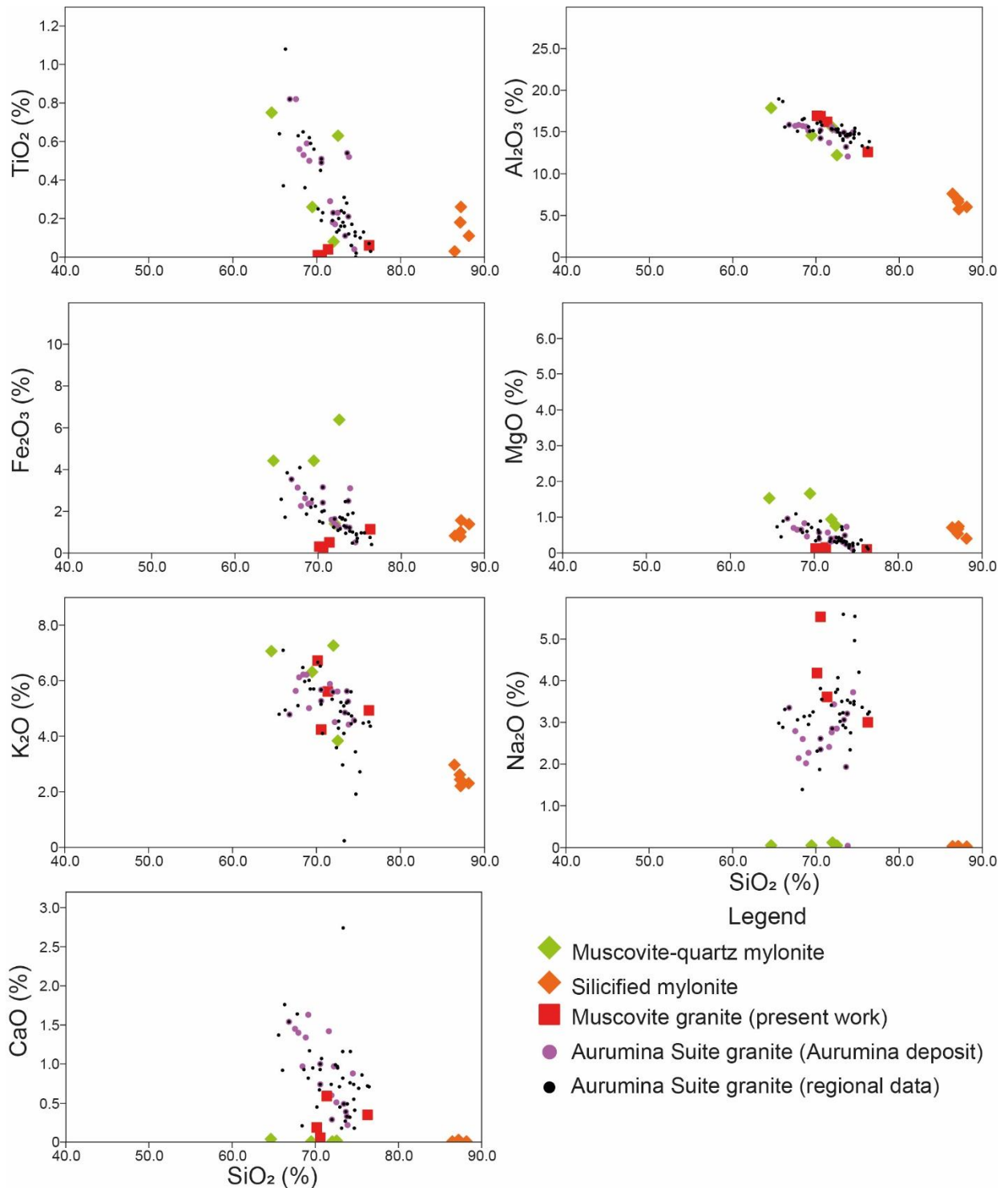
Figure 11. Harker diagrams of major-element oxides vs SiO₂ for granite and mylonite samples.

Chondrite-normalized REE profiles of the average compositions of each rock type are displayed in Fig. 11.REE profiles are defined by lower LREE concentrations for granite from the deposits than those found in both mylonites and average regional data for granite samples of the Aurumina Suite (Fig. 6A). REE patterns in the

muscovite-quartz mylonite from the gold deposits are highly fractionated, with (La/Yb)$_N$ ratio of 25.9, which is higher than the average for granite samples from the deposits, ([La/Yb)]$_N$ of 5.8). REE fractionation patterns of mylonite and granite samples from the deposits are similar and less prominent in relation to those of the average content for regional granite samples of the Aurumina Suite. Silicified mylonite samples have similar fractionation patterns, but with lower REE concentrations caused by the dilution effect due to enrichment in silica. By contrast, muscovite-quartz mylonite samples have global REE contents in general higher than those of granites both from deposits and the regional compilation, particularly in the case of LREEs. Schist samples from the deposits have higher average HREE contents and less fractionated patterns when compared to regional samples, but still displaying relatively HREE-enriched patterns. A negative europium anomaly is observed in all samples, although the anomalies are less pronounced than the average for regional samples for both rock types.
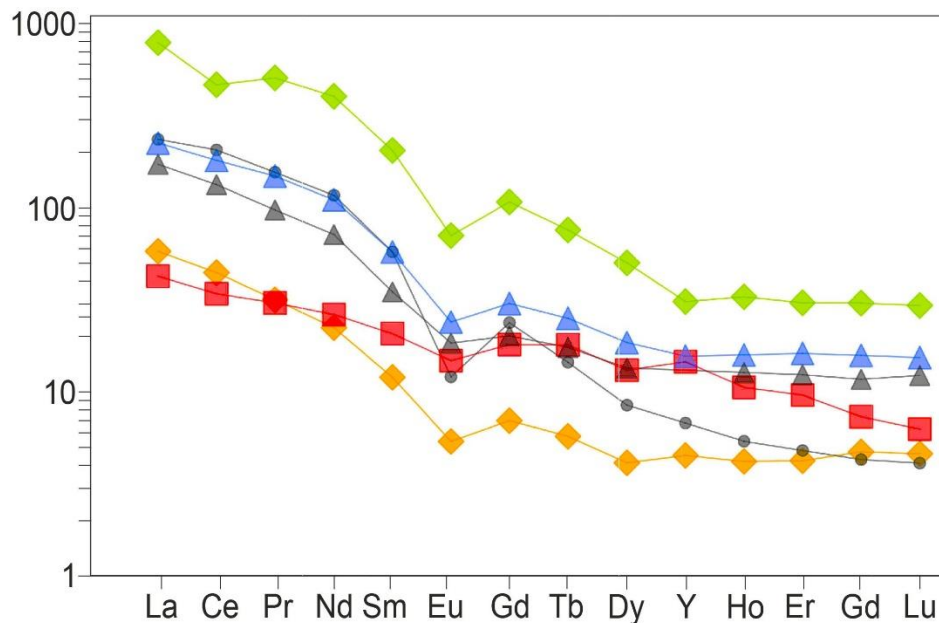
Figure 12. REE patterns of average schist, granite, and mylonite compositions. Legend as in Figure 10. Data normalized to chondrite of McDonough and Sun (1995).

5.2. EPMA

Individual grains of arsenopyrite and chalcocite were analyzed by EPMA for Ag, Pb, Bi, Fe, Cu, Zn, Au, Sb, Co, Ni, S, Se, As, and Te. Results are shown in Table

3. Eighteen analyses were conducted on arsenopyrite from three ore samples of the Novo Horizonte deposit, while twelve analyses were performed on chalcocite grains from two other ore samples, also from Novo Horizonte. Ten disseminated arsenopyrite grains were analyzed in two mineralized mylonite samples, while eleven chalcocite and eight arsenopyrite grains were analyzed in mineralized quartz vein samples, where both minerals are in close spatial association with Au grains.

Sample	Mineral	Element wt. %	Ag	Pb	Bi	Fe	Cu	Zn	Au	Sb	Co	Ni	S	Se	As	Te	Total
99-IV-65_Asp01	Asp-1		0	0.092	0	33.797	0.032	0	0	0.001	0.023	0.089	19.07	0.171	46.745	0	100.02
99-IV-65_Asp02	Asp-1		0	0.043	0	31.589	0.049	0.005	0	0	0.545	1.166	19.256	0.017	46.586	0.093	99.349
99-IV-65_Asp03	Asp-1		0	0.131	0.192	33.123	0.034	0.015	0	0	0.207	0.359	18.568	0.082	47.155	0.099	99.965
99-IV-65_Asp04	Asp-1		0.019	0.117	0.062	32.892	0	0	0.057	0.028	0.015	0.095	19.142	0.105	46.544	0.352	99.428
99-IV-65_Asp05	Asp-1		0	0.022	0	28.608	0	0.02	0	0	0.196	0.435	17.66	0.177	52.544	0	99.662
99-IV-65b_Asp01	Asp-1		0.009	0.193	0.031	33.966	0	0.011	0.042	0	0.036	0.115	19.198	0.093	46.123	0	99.817
99-IV-65b_Asp02	Asp-1		0	0.039	0	33.28	0.026	0.046	0	0	0	0.186	18.805	0.105	46.456	0.129	99.072
99-IV-65b_Asp03	Asp-1		0	0.121	0.012	33.463	0.004	0.007	0.003	0.05	0.078	0.329	18.352	0.106	47.253	0	99.778
99-IV-65b_Asp04	Asp-1		0	0.48	0.043	31.477	0	0	0.032	0	1.029	1.518	19.091	0.135	46.059	0.005	99.869
99-IV-65b_Asp05	Asp-1		0	0.211	0.087	33.624	0	0.085	0.002	0.014	0.171	0.125	18.685	0.048	46.37	0	99.422
NH6_Asp01	Asp-2		0	0.016	0.05	32.33	0.011	0	0	0	0.37	0.441	19.298	0.149	46.591	0.063	99.319
NH6_Asp02	Asp-2		0	0.158	0	33.9	0	0.019	0	0	0.021	0.073	20.112	0	45.696	0	99.979
NH6_Asp03	Asp-2		0.007	0.145	0	33.261	0	0	0.016	0.032	0	0.027	20.592	0.1	45.41	0	99.59
NH6_Asp04	Asp-2		0.013	0.154	0	31.907	0.026	0	0.037	0	0.597	0.444	19.558	0.202	46.898	0.072	99.908
NH6_Asp05	Asp-2		0	0.037	0.07	34.099	0.024	0	0	0.017	0.44	0.16	18.631	0.522	46.122	0	100.122
NH6_Asp06	Asp-2		0	0.117	0.04	33.579	0.05	0	0	0.003	0	0	19.364	0.128	46.417	0.124	99.822
NH6_Asp07	Asp-2		0.007	0.057	0.015	32.68	0	0.054	0	0.075	0.514	0.926	18.117	0.062	47.166	0	99.673
NH6_Asp08	Asp-2		0.006	0.043	0.038	33.07	0	0.033	0	0	0.242	0.253	19.536	0.033	46.618	0	99.872
NH4-V2_Cc01	Cc		0.272	0	0	0.011	78.087	0.093	0.052	0.033	0	0.013	20.542	0.07	0.008	0.01	99.191
NH4-V2_Cc02	Cc		0.249	0.077	0	0	78.674	0.004	0	0.028	0.063	0	20.849	0.158	0	0.088	100.19
NH4-V2_Cc03	Cc		0.558	0.173	0	0.014	77.003	0.167	0	0.017	0	0.013	21.016	0.116	0	0	99.077
NH4-V2_Cc04	Cc		0.099	0.132	0.045	0.029	76.855	0	0.004	0	0	0	21.704	0.129	0.028	0	99.025
NH4-V2_Cc05	Cc		0.36	0.188	0	0.018	78.232	0.016	0.073	0	0	0	20.551	0.163	0.037	0.026	99.664
NH4-V1_Cc01	Cc		0.131	0.03	0	0	78.689	0	0	0.008	0	0	20.15	0.121	0	0.088	99.217
NH4-V1_Cc02	Cc		0.113	0.073	0.113	0	78.417	0	0.055	0	0	0	20.246	0.141	0.054	0.062	99.274
NH4-V1_Cc03	Cc		0.127	0.125	0.016	0.017	77.895	0.028	0.064	0	0	0	20.162	0.155	0	0	98.589
NH4-V1_Cc04	Cc		0.118	0.024	0.082	0.037	78.501	0.134	0.003	0.009	0	0	20.228	0.108	0.034	0.011	99.289
NH4-V1_Cc05	Cc		0.113	0.058	0	0	78.329	0.158	0.047	0	0	0	20.114	0.067	0.026	0.108	99.02
NH4-V1_Cc06	Cc		0.086	0.026	0	0.005	78.382	0.027	0	0.027	0.03	0	20.962	0.068	0	0.222	99.835
NH4-V1_Cc07	Cc		0.13	0	0.062	0	78.528	0.104	0	0.005	0	0	20.246	0.175	0.036	0	99.286

Sample	Mineral	Atomic %	Ag	Pb	Bi	Fe	Cu	Zn	Au	Sb	Co	Ni	S	Se	As	Te	Total
99-IV-65_Asp01	Asp-1		0	0.02428	0	33.0874	0.02753	0	0	0.00045	0.02132	0.0829	32.5234	0.11841	34.1143	0	100
99-IV-65_Asp02	Asp-1		0	0.01141	0	31.1045	0.0424	0.00421	0	0	0.50808	1.09237	33.0304	0.01184	34.1948	0.04008	100
99-IV-65_Asp03	Asp-1		0	0.03484	0.05063	32.6832	0.02948	0.01264	0	0	0.19338	0.33703	31.9168	0.05723	34.6848	0.04276	100
99-IV-65_Asp04	Asp-1		0.00972	0.03116	0.01637	32.5019	0	0	0.01597	0.01269	0.01403	0.08932	32.9508	0.07339	34.2846	0.15224	100
99-IV-65_Asp05	Asp-1		0	0.00597	0	28.8129	0	0.01721	0	0	0.1869	0.41684	30.9849	0.12609	39.4492	0	100
99-IV-65b_Asp01	Asp-1		0.00456	0.05096	0.00812	33.2714	0	0.0092	0.01167	0	0.03339	0.10718	32.7599	0.06444	33.6791	0	100
99-IV-65b_Asp02	Asp-1		0	0.01041	0	32.9526	0.02262	0.03891	0	0		0.17523	32.4369	0.07354	34.2898	0.05591	100
99-IV-65b_Asp03	Asp-1		0	0.03223	0.00317	33.07	0.00347	0.00591	0.00084	0.02267	0.07298	0.30935	31.5945	0.0741	34.8108	0	100
99-IV-65b_Asp04	Asp-1		0	0.12718	0.0113	30.9408	0	0	0.00892	0	0.95763	1.4197	32.6909	0.09386	33.7497	0.00215	100
99-IV-65b_Asp05	Asp-1		0	0.05619	0.02297	33.2204	0	0.07174	0.00056	0.00635	0.15995	0.1175	32.1594	0.03354	34.1514	0	100
NH6_Asp01	Asp-2		0	0.00425	0.01315	31.8266	0.00952	0	0	0	0.34485	0.41306	33.0945	0.10375	34.1903	0.02715	100
NH6_Asp02	Asp-2		0	0.04129	0	32.8654	0	0.01574	0	0	0.01928	0.06734	33.9667	0	33.0243	0	100
NH6_Asp03	Asp-2		0.00351	0.03789	0	32.2477	0	0	0.0044	0.01423		0.02491	34.7794	0.06858	32.8194	0.03085	100
NH6_Asp04	Asp-2		0.00659	0.04064	0	31.2354	0.02237	0	0.01027	0	0.55333	0.41355	33.3538	0.13987	34.2241	0	100
NH6_Asp05	Asp-2		0	0.00978	0.01835	33.4527	0.02069	0	0	0.00765	0.40868	0.14935	31.8409	0.36222	33.7298	0.05316	100
NH6_Asp06	Asp-2		0	0.03089	0.01047	32.8911	0.04304	0	0	0.00135		0	33.0419	0.08868	33.8925	0	100
NH6_Asp07	Asp-2		0.00359	0.01522	0.00397	32.3836	0	0.04571	0	0.03409	0.48223	0.87305	31.2744	0.04346	34.8408	0	100
NH6_Asp08	Asp-2		0.00303	0.01132	0.00992	32.2949	0	0.02753	0	0	0.22375	0.23507	33.235	0.02279	33.9367	0	100
NH4-V2_Cc01	Cc		0.13446	0	0	0.0105	65.5201	0.07585	0.01408	0.01445	0.05638	0.01181	34.1657	0.04727	0.00569	0.00418	100
NH4-V2_Cc02	Cc		0.12185	0.01962	0	0	65.3519	0.00323	0	0.01214		0	34.3292	0.10563	0	0.03641	100
NH4-V2_Cc03	Cc		0.27547	0.04446	0	0.01335	64.5253	0.13602	0	0.00744		0.01179	34.908	0.07823	0	0	100
NH4-V2_Cc04	Cc		0.04854	0.0337	0.01139	0.02746	63.9651	0	0.00107	0		0	35.8066	0.08641	0.01977	0	100
NH4-V2_Cc05	Cc		0.17754	0.04827	0	0.01715	65.4877	0.01302	0.01972	0		0	34.1005	0.10982	0.02627	0.01084	100
NH4-V1_Cc01	Cc		0.06495	0.00774	0	0	66.2261	0	0	0.00351		0	33.6157	0.08196	0	0.03689	100
NH4-V1_Cc02	Cc		0.05601	0.01884	0.02891	0	65.9801	0	0.01493	0		0	33.7671	0.09548	0.03854	0.02598	100
NH4-V1_Cc03	Cc		0.06332	0.03244	0.00412	0.01637	65.9175	0.02303	0.01747	0		0	33.8202	0.10557	0	0	100
NH4-V1_Cc04	Cc		0.05842	0.00619	0.02096	0.03538	65.9711	0.10946	0.00081	0.00395		0	33.6964	0.07305	0.02424	0.0046	100
NH4-V1_Cc05	Cc		0.05617	0.01501	0	0	66.0845	0.12957	0.01279	0		0	33.6378	0.04549	0.01861	0.04538	100
NH4-V1_Cc06	Cc		0.04218	0.00664	0	0.00474	65.2503	0.02185	0	0.01173	0.0269	0	34.5901	0.04556	0	0.09204	100
NH4-V1_Cc07	Cc		0.06434	0	0.01584	0	65.973	0.08493	0	0.00219		0	33.7157	0.11833	0.02565	0	100

Table 3. EPMA data of arsenopyrite and chalcocite in ore samples from the Novo Horizonte deposit, expressed as atomic % and as element weight %.

Analyses of disseminated arsenopyrite (Asp-1) grains showed As concentrations of 33.67–39.45 at. % (average: 34.74 at.%), S concentrations of 30.98–33.03 at.% (average: 32.30 at%) and Fe concentrations of 28.81–33.27 at.% (average: 32.16 at%). Quartz vein-hosted arsenopyrite (Asp-2) grains have lower As contents (32.81–34.84 at.%, average 33.83 at.%), higher S (31.27–34.78 at.%, average 33.07 at.%) and similar Fe concentrations (31.24–33.45 at.%, average: 32.40 at.%) when compared to the arsenopyrite results above. Most arsenopyrite samples contain noticeable amounts of Ni and Co, plus a wide range of other trace elements such as Au, Ag, Cu, Pb, Bi, Se and Te (Table 3). Asp-1 contains up to 1.42 at.% Ni (minimum 0.08, average 0.41 at.%), while Asp-2 contents range between 0.02 and 0.87 at. % (average 0.27 at.%). Co contents were relatively similar between the two arsenopyrite types, with a total average of 0.23 at. %. Cobalt/Nickel ratios are low for both arsenopyrite types (Asp-1 median 0.45; Asp-2 median 0.83), with Co and Ni displaying strong positive correlation (Figure 12B). Other detected trace elements in arsenopyrite include Se up to 0.52 wt.%, Sb up to 0.075%, Pb up to 0.48 wt.%, Te up to 0.35 wt.%, Bi up to 0.19 wt.%, Zn up to 0.15 wt.%, and Cu up to 0.05 wt.%. Asp-1 is slightly more enriched in Bi and Te than Asp-2, while the latter appears to have higher Sb and Se contents.
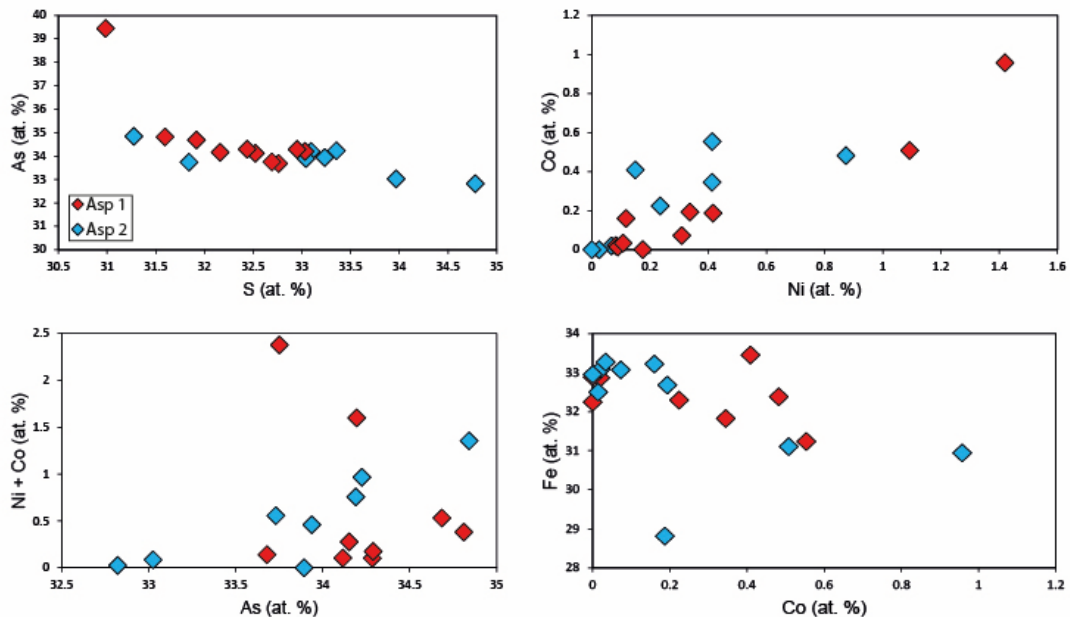
Figure 13. Relationship between concentrations of arsenic and sulfur (A), nickel and cobalt (B) nickel+cobalt and arsenic (C) and iron and cobalt in arsenopyrite of the Novo Horizonte deposit.

Gold contents above detection limited were observed in seven arsenpyrite analysis. Arsenopyrite-1 has an average of 0.014 wt.% Au, with maximum Au contents of 0.057 wt.%, while arsenopyrite-2 has lower Au contents, with an average of 0.007 wt.% and with the highest value being 0.037 wt.%. Au values above detection limit occur in seven chalcocite analysis, with an average value of 0.042 wt.%, up to 0.072 wt.%. Chalcocite analysis also revealed significant Ag values (up to 0.558 wt. %, average 0.172 wt.%).

Arsenopyrite chemical data were used to estimate its temperatures of crystallization according to the geothermometer developed by Kretschmar and Scott (1976) and Sharp et al. (1985). Arsenopyrite analyses containing more than 0.5 atom % Co, Ni, and Sb were not used for geothermometric purposes. Analyses show little variation of As/S atomic ratios between them, with overall values between 0.97 and 1.06, and average value of 1.03. The global Fe variation is within 1 wt.%, complying with the requirements for the use of this geothermomether. As values range from 33.7 to 34.3 for Asp–1, and from 33 to 33.9 for Asp–2. When plotted in the arsenopyrite geothermomether diagram (Fig. 13), the data indicate possible temperatures in a global range of 390-535 °C. For Asp-1, minimum and maximum temperatures must range from 425 to 510 °C and from 460 to 535 °C, respectively. Asp-2 data indicate minimum and maximum temperatures between 390-480 °C and 435-520, respectively.
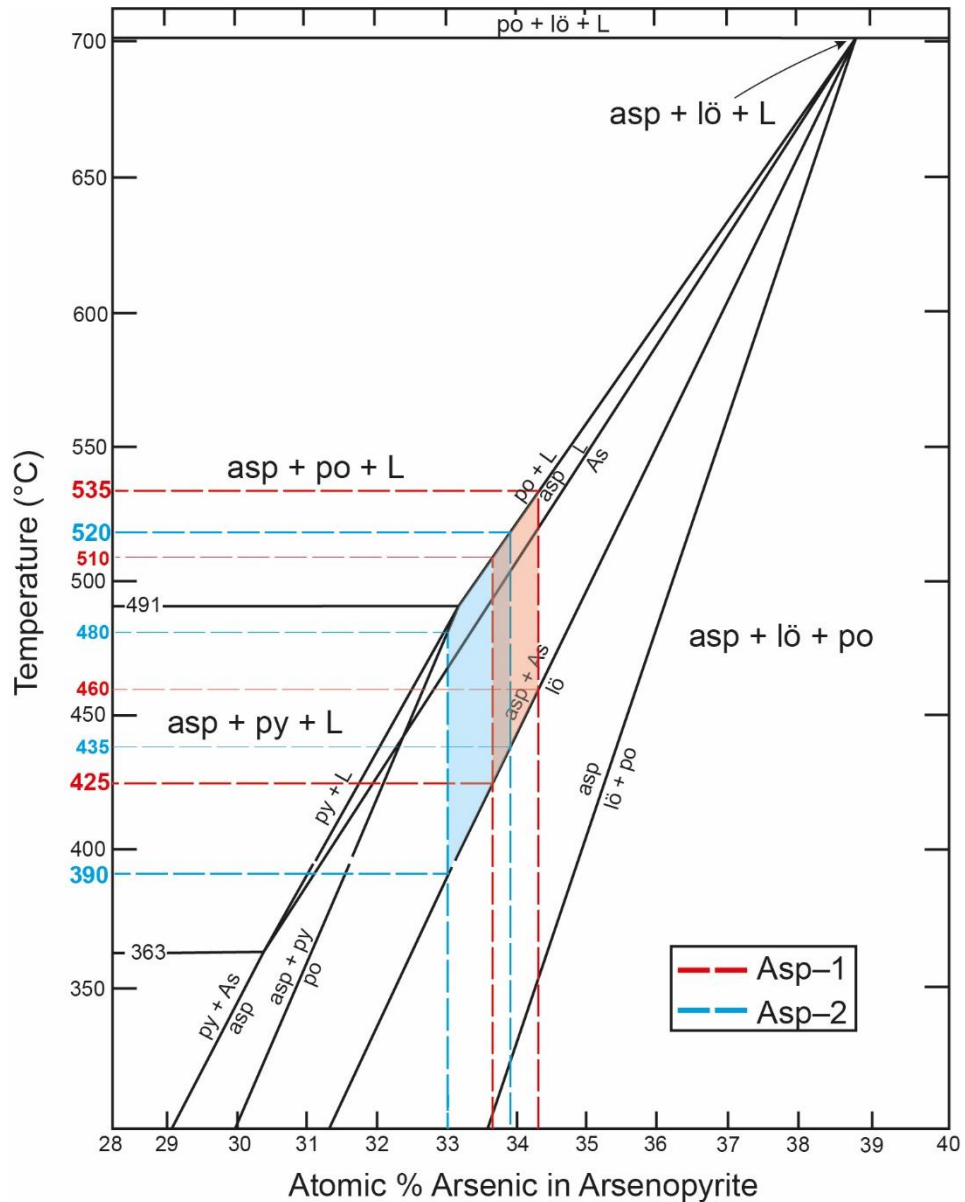
Figure 14. Temperature estimates from Atomic % of As in arsenopyrite, based on the phase diagram of Kretschmar and Scott (1976). asp = arsenopyrite, lö = löllingite, po = pyrrhotite, py = pyrite, L = liquid, As = native arsenic.

5.3. Sulfur isotopes

A total of 18 spots were analyzed in situ including 8 spots on pirite and 10 spots on arsenopyrite in a mineralized vein sample from the Novo Horizonte deposit. Bulk dissolved sulfide analysis were performed on three sulfide samples from the Aurumina mine, of sphalerite, pyrrhotite and pyrite. The range of $\delta^{34}S$ ratios for arsenopyrite varies from -5.62 to -1.76‰ (Fig.14). $\delta^{34}S$ ratios for pyrite range

between +0.53 and +9.98‰ (Fig.14). The mean $\delta^{34}S$ ratios of arsenopyrite is -3.68‰, lighter than the mean of pyrite (+4.19‰). Sulfide samples from the Aurumina deposit yielded bulk $\delta^{34}S$ values of -4.7‰ for sphalerite, -5.1‰ for pyrrhotite, and -6.4‰ for pyrite.
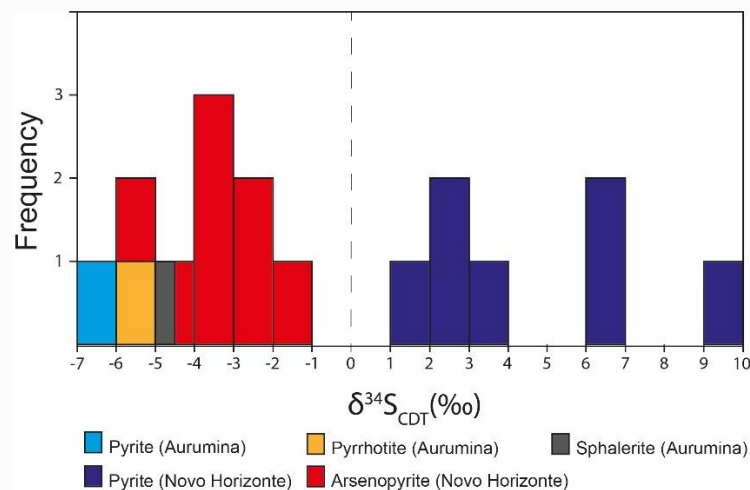
Figure 15. Frequency vs. $\delta^{34}S$ ratios histogram for arsenopyrite and pyrite from Novo Horizonte.Ranges of pyrite, pyrrhotite and sphalerite from the Aurumina deposit are also shown for comparison.

6. Discussion

6.1 Sources for the mineralizing fluids

Considerations over the origin of gold and other metals in the studied deposits unavoidably regard either granitic or graphite-bearing schist host rocks as a possible source, at least initially. The likely protolith for the schist is thought to be similar to black shales. A seawater source, in an anoxic sedimentary environment with organic matter deposition has been attributed as a source for Au, Ag and PGE enrichment in black shales of various ages and locations, including associations with Ni, Co, Cu, and base metals (Holland, 1979; Meyers et al., 1992; Pašava, 1993; Xu et al., 2013; Pagès et al., 2018; Fu et al., 2021). Processes responsible for this enrichment in the schist protolith would be linked to the redox reactions arising from high biogenic activity, as suggested by the high amount of organic carbon in the schist, that could

directly cause precipitation of redox-sensitive metals from O_2-depleted ocean water (Piper, 1994; Rimmer, 2004). These reduced deep basinal H_2S-rich fluids may carry Au (± As, PGE, U) along with other trace elements, including Ni, Co, Se, Te, Ag, Cu, Pb, and Zn. Such fluids would then interact with sea-floor organic-rich sediments and lead to the formation of syngenetic to early-diagenetic sulfide.

Variations in major element contents are within the same range as those of schist samples from Cuadros et al. (2017b), with some samples showing higher $TiO2$, Fe_2O_3 and MgO. When comparing the results of Ticunzal Formation schist geochemical analyses from the gold deposits with average values of available Ni, Sc, Th, Zr, and REE data for schist samples (n=26) obtained from Cuadros et al. 2017b), some differences are observed, as for example, slight Ni (40 vs 22 ppm), and HREE enrichments (Fig. 11), probably related to protolith composition. Cobalt and nickel contents are more likely controlled by the original Co and Ni endowment of the hydrothermal fluid, rather than by physico-chemical conditions at the precipitation site, as sulfarsenides can precipitate over a broad range of fS_2 and redox conditions (Scharrer et al., 2019). The origin of relatively Ni- and Co-enriched arsenopyrite and chalcocite that occur at Novo Horizonte is much more plausibly related to schist compositions than to those of granite samples, as those elements are several times more abundant in schist samples when compared to granite, both at the deposit and regional scales. Co/Ni ratios from higher-temperature arsenopyrite also suggest that graphitic schist could have acted as a source for these metals, particularly in the case of sulfides interpreted to form first.

The processes by which metals could later be mobilized to form hydrothermal gold deposits are metamorphic devolatilization, magmatic assimilation followed by transferring to exsolved fluids, and wallrock leaching. During regional metamorphism of these rocks, metal scavenging and their incorporation to fluids can be achieved at depths of greenschist-amphibolite facies transition zone conditions, with dehydration of chlorite being able to extract metals such as Au, Cu, Pb, and Zn, coupled with release of aqueous-carbonic fluids capable of complexing and transporting metals bounded to organic carbon (Zhong et al., 2015). Atypical Au-Cu-Co-Ni metallic associations in gold deposits from the Pohjanmaa Belt (Hector et al., 2023), and local variations in metal contents among deposits belonging to the same structural system are attributed to metamorphic Au ore-forming fluids with lithologically diverse sources over time. Interpretations on the origin of sulfur and Au in Archean orogenic Au

deposits favor a deep-seated source, instead of a local reservoir at the site of gold precipitation (LaFlamme et al., 2018). Metals could have also been partially derived from interactions between country rock and fluids exsolved from reduced magmas, with devolatilization reactions that take place at the contact aureoles of the intrusions being in some cases responsible for fluid mixing, formation of late silver- and base metal-veins that also contain gold, and shifting of sulfur isotopic signatures (Mair et al., 2006, 2000; Marsh et al., 2003). Regarding the Ticunzal Formation graphite-bearing schist as the reservoir provider of metals either at the source of the fluids or at the wall-rock interaction sites of deposition, diversities in metal-sulfide parageneses between the deposits could be explained by variations in the sedimentary input and ocean chemistry occurring at different portions of the sedimentary basin at different times during sediment accumulation. Differences could also arise from varying degrees of interaction between fluids and country rocks during both magmatic and hydrothermal processes. This may explain the PGE enrichment observed in some of the deposits, and differences in sulfide species and their respective abundances, such as the pyrite-only paragenesis at Morro dos Borges, and the more conspicuous Cu, Pb and Zn sulfide assemblage in veins from the Aurumina and Novo Horizonte deposits.

There is no clear correlation between As and Au contents of granite and schist samples, neither in the deposits studied in this work nor in the Aurumina and Buraco do Ouro deposits, which suggests that higher As concentrations are not directly related to higher Au grades. Comparing to other trace elements, gold only shows some degree of correlation with Cu, Pb and Zn in a few mineralized quartz vein samples, with no widespread covariance relationship observed. While these elements may be indicators for gold mineralization, gold also occurs in sulfide-poor to sulfide-absent parageneses, with varied metallic contents. Sulfide content is even lower in the Tucano and Morro dos Borges deposits, although minor amounts of arsenopyrite and pyrite can still be found closely related to gold mineralizations. In the Buraco do Ouro deposit, however, sulfides are very scarce, and a transport mechanism for gold and PGE via hydroxide complexes in a low-salinity aqueous fluid is suggest instead (Stefánsson and Seward, 2003; Menez, 2014). $Au(OH)^0$ is not considered to play a significant role in gold transport if other ligands are present in the ore-transporting hydrothermal fluid (Seward, 1991a), so the gold transport mechanism might have changed depending on sulfur availability in each case.

Large variations in $\delta^{34}S$ ratios in hydrothermal systems are often interpreted as an indication that sulfur was derived from sedimentary rocks, where biogenic sulfur displays a wide range of $\delta^{34}S$ ratios due to the influence of microbial sulfate reduction (Hutchison et al., 2020; Ohmoto, 1972). Sulfate-reducing bacteria are active in anoxic environments, such as the one proposed for the Ticunzal Formation basin, where H_2S can be fixed either as sulfide minerals or as organic-bound sulfur depleted in ^{34}S relative to the remaining dissolved sulfate. These variations in $\delta^{34}S$ ratios can also derive from slight variations in the fO_2 and/or pH of ore-forming fluids during ore deposition. In a solution that contains no sulfate, the $\delta^{34}S$ ratio of pyrite might be slightly higher than that of the original fluid at the beginning of deposition, and decrease progressively as a function of minor fluctuations in fO_2 values (Zheng and Hoefs, 1993). This could explain departures in $\delta^{34}S$ ratio differences between arsenopyrite and pyrite in mineralized quartz veins from Novo Horizonte. Considering that early arsenopyrite did not form with coeval pyrite, it would preferentially incorporate the lighter sulfur isotope when compared to pyrite formed later at more oxidizing conditions. If variations in $\delta^{34}S$ ratios of pyrite from Novo Horizonte are accounted for this process, other values remain relatively uniform among the Novo Horizonte, Aurumina and Buraco do Ouro deposits (Fig. 15), from slightly more negative ratios for bulk pyrite from Aurumina to +2-5‰ for guanajuatite (Bi_2Se_3, with minor Se replacement by S) from Buraco do Ouro (Menez, 2014), though comparison is limited due to different analytical methods. Precipitation of the ^{34}S-enriched pyrite may have also resulted from a fluid with a different composition, possibly with greater wallrock contribution. The relatively wide total range of $\delta^{34}S$ ratios (16.4‰) among the deposits, from a minimum of -6.4‰ for pyrite at Aurumina to a maximum value of nearly +10‰ for pyrite from Novo Horizonte, is difficult to explain solely by changes in physico-chemical conditions during different stages of ore mineral precipitation. This range could be even larger considering that total isotopic ratios obtained for bulk dissolved sulfide from Aurumina could represent an average of a composition with considerable internal heterogeneities. Besides, the diversity in metal enrichment between the studied deposits most likely imply that the respective ore fluids had different metal contents during metallogenic evolution.

Hydrothermal systems associated with more reduced magmas are dominated solely by H_2S instead of a having significant proportions of both H_2S and SO_2, and thus generally show less sulfur isotopic variations because SO_2 is not present in the

fluids (Burnham and Hiroshi, 1980). Crustal contamination of the magmas can cause variations in sulfur isotopic compositions of magmatic-hydrothermal systems, and thermal aureoles around granitic intrusions can induce devolatilization of country rocks that contribute with a generally wider isotopic range of supplied sulfur. Devolatilization of a pelitic rock containing a graphite-pyrite-pyrrhotite assemblage can provide a mechanism for transferring sulfur from country-rock into a pluton, without requiring bulk assimilation of material, as experimentally shown by Poulson and Ohmoto (1989), if pelite is raised to temperatures >400°C, but less than the melting temperature. Hence, incorporation of country rock sulfur could have occurred, while also possibly mobilizing ore-forming metals as sulfide complexes. Exsolution of fluids having the observed $\delta^{34}S$ signature may have occured directly from granitic magma that has been previously contaminated and incorporated S from country rock through mechanisms of physical xenolith disaggregation and chemical dissolution (Woods, 1992). Generally, sulfides with sulfur derived from magmatic fluids have $\delta^{34}S$ ratios between 0 and +5‰ (Huston, 1999). Ishihara and Sasaki (1989) attributed slightly negative values of around -4.5‰, found in ilmenite-series granitoids of the Sierra Nevada batolith, to incorporation of sedimentary sulfur enriched in ^{32}S at the site of magma generation, instead of the site of emplacement. Rocks of either the Ticunzal Formation or another possible metasedimentary sequence could have contributed this way as sources of sulfur. The widespread presence of paragneiss and graphite schist xenoliths in granites of the Aurumina Suite further suggests that sulfur could have been transfered to granitic magma via xenolith digestion. Granite samples from Novo Horizonte show slight Pd and Pt enrichment, with similar Au/Pd and Pd/Pt ratios as granite samples from Buraco do Ouro (Menez, 2014), where they are also probably related to assimilation of graphite schist xenoliths.
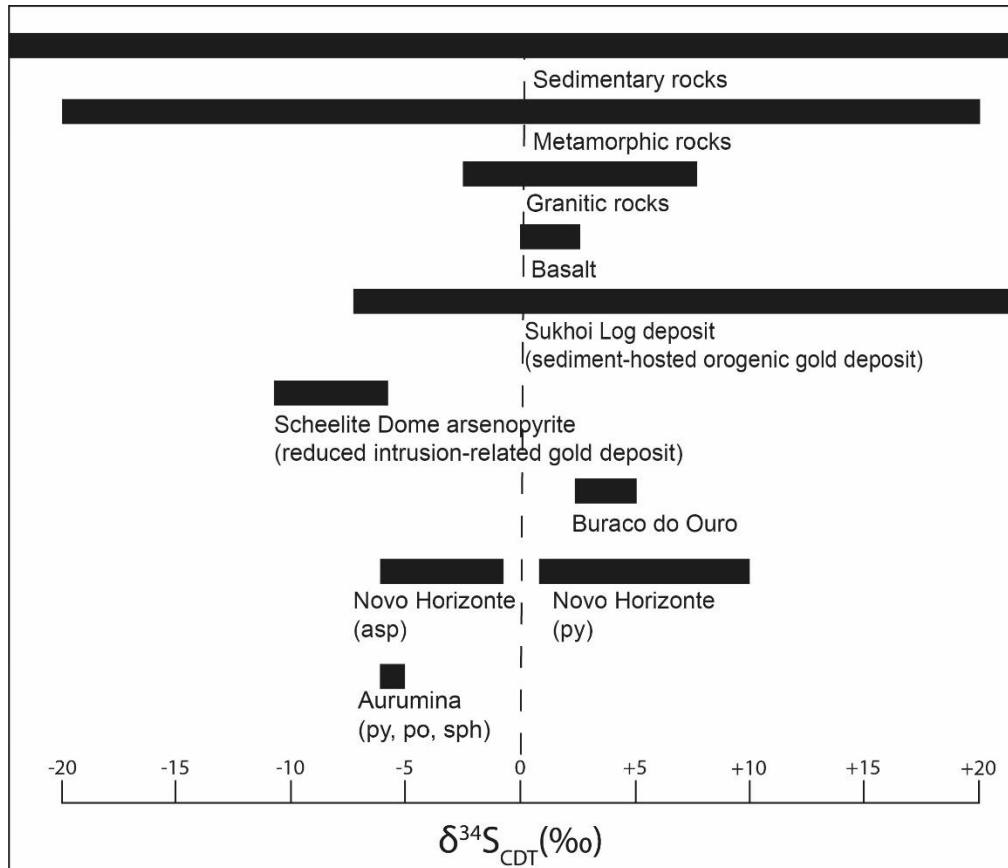
Figure 16. Isotopic composition of sulfur from sulfides of the Novo Horizonte, Aurumina and Buraco do Ouro deposits compared to data compiled for different sulfur reservoirs (data from Seal, 2006), the Scheelite Dome reduced intrusion-related gold deposit (Mair et al., 2000) and a black shale-hosted orogenic gold deposit (Sukhoi Log deposit, Chang et al., 2008). Asp: arsenopyrite; py: pyrite; po: pyrrhotite; sph: sphalerite.

6.2 Ore-forming processes

The region encompassing the deposits consists of a NE-SW trending domain (Fig. 4) varying to NNE-SSW and E-W, with an average width of 28 km and a contrasting magnetic texture as seen in analytical signal inclination maps (Serafim, 2017). Local variations in fluid flow associated with the development of the S foliation and/or deflections in the regional foliation strike, could have acted as lower-order structural traps with repetitive sigmoidal geometries recognized in aeromagnetic data, limited by E-W lineaments. These sigmoidal features have a fractal nature at district, deposit, outcrop and microscopic scales. Structural control of the mineralizations consists of shear zone networks and S-C fabric at all scales, and also of continuous structures (Blenkinsop et al., 2020) with individual features at deposit

scale such as S-C fabric and veins. Veins themselves actually represent elongate orebodies with geometries defined by the fabric. The lensoid and discontinuous geometries may reflect the degree of transposition and dismemberment along the S foliation. The control associated with the formation of auriferous silicified lenses along the shear zones could thus result from hydrothermal fluid permeating along cooling margins of plutons, being exsolved either from the latter or from deeper sources, and accumulating preferentially in specifc favourable sites, such as zones where the orientation of the fault becomes oblique to the regional slip vector.

Emplacement of granitic magma was also controlled by regional transpressional kinematics along the two lithospheric-scale boundary faults, while the structures were active. The syn-tectonic nature of the magmatism is inferred from *lit-par-lit* structures where Aurumina Suite monzogranite intruded Ticunzal Formation paragneisses and schists along mylonitic foliation planes, having imprinted the same pervasive mylonitic foliation in both granites and country rocks (Cuadros et al., 2017a). Several works invoke causative links between magmatism and shear zones, with the latter commonly controlling ascent and emplacement of magma (Brown and Solar, 1999; Petford, 2003; Cruden and Weinberg, 2018). Furthermore, available geochronological data suggest that the earliest intrusions of the Aurumina Suite occurred at nearly the same time as peak metamorphic temperatures of the Ticunzal Formation were achieved, during a short time window after deposition of sediments (2.15-2.16 Ga for the earliest magma pulses, and 2.16-2.19 Ga for the deposition interval). Raman spectroscopy analyses of high-crystallinity graphite from the schist indicate peak metamorphic temperatures of 620-630°C (Cuadros et al., 2017b). The thermal disturbance induced by the Aurumina Suite magmas, and the elevated geothermal gradient associated with astenospheric upwelling regarded to have caused this magmatism (Cuadros et al., 2017a), could have played a role in attaining amphibolite facies conditions.

Gold and electrum in the deposits are mainly visible, occurring as inclusions in arsenopyrite and pyrite grains and at the interstices between hydrothermal muscovite lamellae. The strong relation of gold and muscovite indicates a gold-muscovite association where generation of muscovite is clearly related to gold mineralization in a hydrothermal mica-quartz-gold-sulfide system. Examination of the relationships between gold and sulfide assemblages among the studied deposits indicates that there were at least two main stages of gold mineralization. First, precipitation of Au-

As (± PGE, U) at mid- to upper-greenschist facies, where more Ni and Co-enriched arsernopyrite precipitated, probably enriched in invisible Au or Au inclusions. The chemical compositions of arsenopyrite reveal that there is a negative correlation between arsenic and sulfur, consistent with the substitution $FeAs_{1\pm x}S_{1\pm x}$ (Abraitis et al., 2004), indicating chemical equilibrium during the formation of various arsenopyrite grains that yielded different temperature estimates. The earlier arsenopyrite grains show frequent dissolution textures (Fig. 9D), as well as minor Au contents slightly higher than those of later arsenopyrite. Afterwards, an ore assemblage consisting of coexisting (but not necessarily coeval) native gold (as both free grains and electrum in Aurumina and Buraco do Ouro), arsenopyrite, pyrrhotite, chalcopyrite, galena, sphalerite and pyrite formed in quartz (plus carbonate, only at Aurumina) veins, probably following later remobilization processes in mid-greenschist facies. This is in line with the characteristics observed in the mineralized veins at the Aurumina deposit, namely structural elements typical of brittle regime, enrichment in Ag, Pb and Zn, and temperatures inferred from the arsenopyrite geothermometer (315-373°C) of grains in mineralized veins from Aurumina (Cunha, 2006), that are lower when compared to those of Novo Horizonte (390-535°C, in total). Structures observed at Aurumina include brecciated zones in the veins and thick pockets of barren milky quartz filling up extension fractures associated with the system that generated the mineralized veins, parallel to the regional (or "C") foliation. A sulfur isotope geothermometer applied to the pyrite-sphalerite and pyrite-pyrrhotite pairs (Kajiwara et al., 1969; Kajiwara and Krouse, 1971) for the Aurumina deposit yielded equilibrium temperatures of 147°C and 207°C, respectively, highlighting the protracted thermal history of this deposit. Fluctuations in fluid pressure may explain contrasting geometries of orebodies within the same deposit and also between deposits (Blenkinsop et al., 2020), so more disseminated ore in muscovite-quartz mylonite and vein-hosted gold may form during episodes of pressure decrease, while fluid interaction with chemically reactive graphitic schist wallrock provides a destabilization mechanism of gold-sulfur complexes through sulfidation of Fe-bearing minerals as well as graphite-related reduction (Seward, 1991). Ductility of wallrocks could have initially inhibited more channelized fluid flow, resulting in pervasive flow and disseminated sulfide precipitation, while veins formed at later stages of lower temperature.

6.3 Classification

Several characteristics of the gold deposits allow to classify them as part of either orogenic or reduced intrusion-related gold systems. Features that are common to both types include tectonic setting, mineralogy and geometry of alteration haloes (narrow silicification and sericitization zones), metal association, reduced sulfide parageneses, low sulfide content, temperatures of formation, and even spatial and temporal association with granitic intrusions (Groves et al., 1998; Lang and Baker, 2001; Goldfarb et al., 2001; Goldfarb and Pitcairn, 2023). Characteristics of reduced intrusion-related gold systems (RIRGS) largely overlap with those of orogenic gold deposits, but they also have a unique combination of genetic links to magmatism that justifiy their separate classification (Lang and Baker, 2001). The genetic model proposed by Hart (2007) is based on the nature of fluids exsolved from the cooling intrusion, which migrate to the cupola region and react with adjacent country rocks to form mineralizations. RIRGD ores are commonly located in provinces known for Sn-W occurances, in foreland regions of orogens where felsic magma was intruded within sedimentary sequences deposited at old continental margins, inland of plate boundary and accreted-terrane collisional zones (Lang et al., 2000; Thompson et al., 1999). This specific continental arc setting is similar to the one suggested for the Aurumina Suite magmatism by Cuadros et al. (2017a), and a regional Sn (±W) endowment also occurs in the area (e. g. Botelho and Moura, 1998; Moura et al., 2014; Santos et al., 2023). The metal associations inferred from enrichments identified in chemical analyses, including As-Te-Bi-Sb, and Ag-Cu-Pb-Zn, are comparable to those of both deposit types. In intrusion-related gold deposits, Au-Te-Bi±As assemblages are typical of intrusion-hosted mineralizations, while Au-As-Sb and more distal Au-As-Sb±Ag±Pb±Zn assemblages occur in thermally-metamorphosed country rocks (Groves et al., 2003; Lang et al., 2000; Lang and Baker, 2001). Enrichments in these elements are observed in the studied deposits, but withou the spacial distributions described above. Orogenic gold deposits typically have fairly similar Au-As-B-Bi-Sb-Te-W associations (Goldfarb and Groves, 2015).

The structural control of orogenic gold deposits is ultimately related to crustal-scale fluid focusing first-order faults of convergent margins (Groves et al., 2020), with metamorphic fluids being progressively released either from devolatilization of supracrustal successions underlying the host rocks of the deposits or from

devolatilization of a subducted slab and overlying sediment wedges (Groves and Santosh, 2016). Fluids are channelized through secondary faults of regional shear zones either during or immediately after peak metamorphism (Groves et al., 1998, 2020). The dominant structural control on RIRGS, on the other hand, is related to pluton emplacement, movement of magma and hydrothermal fluids, which define a dominant direction that may be important for later localizing of mineralizations (Hart, 2007). Shear-hosted veins in plutons are found in RIRGS, filling structures that were active during emplacement (Stephens et al., 2004). Some orogenic Au deposits exhibit close spatial and temporal relationships with granite intrusions, but have inconsistent and equivocal genetic relationships (Goldfarb and Groves, 2015; Goldfarb and Pitcairn, 2023). A common role invoked for the intrusions in deposits of this type is that of a structural component, acting as rigid bodies that cause heterogeneities in the local stress field relative to the regional field, creating anomalous minimum stress zones that favour fluid deposition (Groves et al., 2018).

There is no unequivocal interpretation of available data as to whether the ore-forming fluids had a magmatic or metamorphic source. The relatively large variability in $\delta^{34}S$ ratios of sulfides is considered to be inherited from source rocks, with processes at the deposition site possibly influencing to a limited extent. Reported $\delta34S$ ratios of sulfides from orogenic-type mineralizing fluids vary from −20 to +25‰, and cluster around 0-+10‰, thus placing them as hypothetically feasible sources, although there is no unique signature attributed to them (Goldfarb and Groves, 2015). Considering extensive documented an experimental links established between organic matter sedimentary accumulation and metal (including gold) enrichment (e. g. Gaboury, 2021; Xu et al., 2013), Ticunzal Formation graphite-bearing schist would seem to be a likely source for gold through metamorphic devolatilization, forming an orogenic-type gold deposit. The strong structural control and apparent protracted mineralization period are also characteristics of orogenic gold deposits. Fluids would then deposit in favourable structural sites of granite margins, aided by interaction with chemically reactive graphite schist. But several problems arise if Ticunzal rocks are considered as direct sources, and if the deposits are considered as orogenic-type. The fact that Ticunzal Formation rocks reached upper amphibolite facies conditions complicates a direct association, since metamorphic devolatilization models for orogenic Au-bearing fluids point to a source at depth, not at the deposition site, from rocks at that same metamorphic grade

(Goldfarb and Groves, 2015; LaFlamme et al., 2018). In a supracrustal orogenic gold source model, the metamorphic fluid derived from devolatilization occurring at the greenschist- to-amphibolite-facies transition is transported later to higher crustal levels and deposited in rocks metamorphosed during the same metamorphic event, but at lower metamorphic grades. Therefore, the fluid source must have been located at a depth greater than that of deposit, and deposits hosted in amphibolite-facies rocks would be anomalies in this model (Goldfarb et al., 2001; Goldfarb and Groves, 2015; Groves and Santosh, 2016). Besides, even fluids were considered to have originated from other sources, but still as orogenic-type, such as devolatilization of a subducted oceanic crust and overlying sediments (Goldfarb and Groves, 2015), granite intrusions would not necessarily have an essential contribution apart from acting as rheologically competent barriers, which does not appear to be the case. The fact that there are no gold mineralizations hosted in schist with no granitic rocks present, and that magma emplacement also occurred during shearing, along with the mineralization control associated with transpressive shear-zone dynamics demonstrated by the geometry of orebodies and fabric of host rocks, point to a fundamental role for intrusions in the deposit formation. These evidences imply that the mineralizations are dependent on the presence of granitic intrusions, favoring an intrusion-related origin despite ambiguities presented by geochemical and mineralogical charateristics that are shared between deposit types.

Some of these ambiguities may be intrinsic characteristics of the magma source and later fluid-related processes. The discussed mechanisms responsible for the observed isotopic variability could have acted combined; i.e., exsolution of fluids from a reduced magma that had previously assimilated metasedimentary rock at the source or during transport, interaction of those fluids with graphite-bearing schist and gradual fO_2 variations at the sites of deposition, with later pulses of hydrothermal activity remobilizing gold. Previous deposition of Ticunzal Fm. Sediments occurred in a continental arc-related basin, at the western margin of the Sao Francisco Craton during the Rhyacian (Fig.17A). A hybrid source for the Aurumina Suite magma through interaction of a mantle-derived basaltic melt with metasedimentary rocks (Fig. 17B) is proposed by Cuadros et al. (2017a) based on geochemical and Nd isotopic data, which would be in agreement with a reduced magmatic-hydrothermal source for the fluids displaying a mixed sulfur isotope signature of magmatic and metasedimentary rock reservoirs. Therefore, a magmatic-hydrothermal model is

reasonable, in a RIRG system where intrusion-hosted type mineralizations were synchronous to shearing, with significant contribution from metasedimentary rocks at the source of the magma, and likely with contribution from graphite-bearing schists of the Ticunzal Formation during transport and emplacement (Fig. 17C).
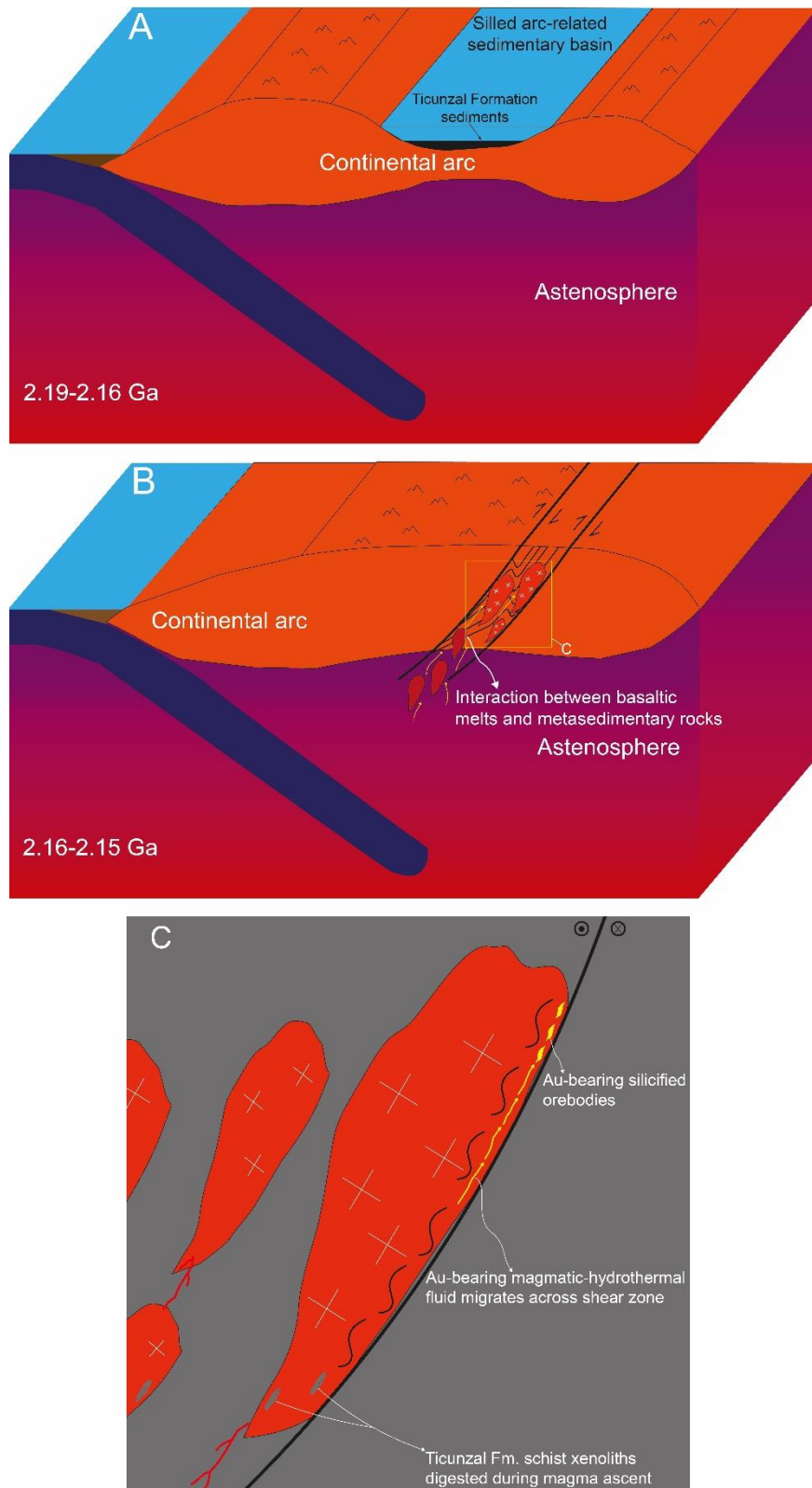
Figure 17. Schematic diagrams depicting the evolution of the tectonic and magmatic-hydrothermal system of the gold mineralizations associated with the Aurumina Suite. A. Deposition of Ticunzal Formation sediments in a in a silled, restricted basin related to a continental arc setting. B. Onset of Aurumina Suite magmatism through interaction of mantle-derived basaltic melts and metasedimentary rocks. C. Migration of granitic magma through fault systems with incorporation of graphite-bearing schist

xenoliths during ascent, exsolution of magmatic-hydrothermal fluids from the magma and precipitation of gold in the contact zone during shearing, forming silicified, sigmoidal orebodies and fault-parallel quartz veins.

7. Conclusions

The studied gold mineralizations are, without exception, located at the sheared contact zone between reduced, peraluminous Aurumina Suite granites and Ticunzal Formation graphite-bearing schists,. Structural elements controlling the gold mineralizations are recognized through interpreted magnetic data, and consist of NE-SW fault system boundaries with associated fractal, repetitive sigmoidal features that are spacially related to Au occurrences. The main structural control is associated with development and evolution of a mylonitic S-C fabric, forming either S foliation-parallel sigmoidal muscovite-quartz mylonite orebodies or C foliation-parallel quartz veins.

Although the deposits share similarities in conditions and sequence of mineralization events, they do not show the same metal endowment which suggests different mineralizing conditions and variations in the source of the fluids, or, to a lesser extent, wallrock input at deposition sites. If Ticunzal Formation graphite schist is considered as one of the sources of the fluids, variations in sedimentary input during deposition of the protolith could explain spatial variability in compositions through the whole sedimentary sequence. Different temperature ranges for sulfide precipitation were also obtained from geothermometers for different deposits and mineralization styles. Variations in mineralization styles and ore parageneses indicate that sulfides and gold precipitated in at least two stages. Solubility of gold and sulfides decreased through time and deposition was achieved through fluid-wallrock reactions, due to the changes in physicochemical parameters, including fO_2, and late decreases in pressure and temperature. Gold could have been transported by HS^- or OH^- ligands, depending on the sulfur availability of the fluid. Variations in oxygen fugacity of the fluids possibly caused the differences in $\delta^{34}S$ ratios of arsenopyrite and pyrite at Novo Horizonte, but differences in $\delta^{34}S$ ranges observed among the deposits are unlikely to be explained solely by variable precipitation conditions. Ranges obtained are compatible with a sulfur source corresponding to either reduced granitic magma contaminated with country rock, or metamorphic rocks located at variable depths.

The gold deposits exhibit characteristics similar to those of both reduced intrusion-related gold systems and structurally- (shear zone) controlled orogenic gold deposits. However, significant characteristics place the deposits within the category of reduced intrusion-related gold systems, including the tectonic setting of the Aurumina magmatism, location in a Sn mineralization province, the absence of gold mineralizations hosted in schist and unrelated to granitic intrusions and structures indicating coeval magma emplacement and shearing, which is related to the structural control of the mineralizations that share the same deformation fabrics. Therefore, it is plausible to conceive the deposits as part of such system, with contribution from metasedimentary rocks at the source of the magmas and wallrock input via fluid-rock interaction.

8. References

Abraitis, P.K., Pattrick, R.A.D., Vaughan, D.J., 2004. Variations in the compositional, textural and electrical properties of natural pyrite: a review. Int J Miner Process 74, 41–59. https://doi.org/https://doi.org/10.1016/j.minpro.2003.09.002

Almeida, F.F.M., Hasui, Y., Brito-Neves B.B., Fuck, R.A., 1981. Brazilian structural provinces: an introduction. Earth Sciences Review 17, 1–9.

Alvarenga, C.J.S., Botelho, N.F., Dardenne, M.A., Lima, O.N.B., Machado, M.A. 2007, 2007. Geologia das folhas Monte Alegre de Goiás (SD.23-V-C-III), Cavalcante (SD.23-V-C-V) e Nova Roma (SD.23-V-C-VI), Escala 1:100.000.

Blenkinsop, T., Oliver, N., Dirks, P., Nugus, M., Tripp, G., Sanislav, I., 2020. Chapter 1 Structural Geology Applied to the Evaluation of Hydrothermal Gold Deposits. Economic Geology 21, 1–23. https://doi.org/10.5382/rev.21.01

Botelho, N., Fuck, R., Dantas, E., Henrique Laux, J., Junges, S., 2006. The Paleoproterozoic peraluminous Aurumina granite suite, Goiás and Tocantins, Brazil: geological, whole rock geochemistry and U-Pb and Sm-Nd isotopic constraints. The Paleoproterozoic Record of the São Francisco Craton, Ouro Preto, Brasil, Field Guide and Abstracts.

Botelho, Nilson, Moura, M.A., Peterson, R.C., Stanley, C.J., Silva, D.V.G., 2006. Kalungaite, PdAsSe, a new platinum-group mineral from the Buraco do Ouro gold mine, Cavalcante, Goiás State, Brazil. Mineral Mag 70, 123–130. https://doi.org/DOI: 10.1180/0026461067010318

Botelho, N.F., Alvarenga, C.J.S., Menezes, P.R., D'El-Rey-Silva, L.J.H., 1999. Suíte Aurumina: uma suíte de granitos Paleoproterozóicos, peraluminosos e sin-tectônicos na faixa Brasília. VII Simpósio de Geologia do Centro-Oeste e X Simpósio de Geologia de Minas Gerais, Brasília. Abstract volume. 17.

Botelho, N.F., Fonteilles, M., 1992. Les ensembles granitiques subalcalins à péralumineux minéralisés en Sn et In de la sous-province Parana, Etat de Goias, Brésil : (Paragenèses hydrothermales associées : micas lithinifères, helvite, cassitérite et minéraux d'indium).

Botelho, N.F., Moura, M.A., 1998. Granite-ore deposit relationships in Central Brazil. J South Am Earth Sci 11, 427–438. https://doi.org/https://doi.org/10.1016/S0895-9811(98)00026-1

Brito Neves, B.B., 2011. The Paleoproterozoic in the South-American continent: Diversity in the geologic time. J South Am Earth Sci 32, 270–286. https://doi.org/10.1016/J.JSAMES.2011.02.004

Brown, M., Solar, G.S., 1999. The mechanism of ascent and emplacement of granite magma during transpression: a syntectonic granite paradigm. Tectonophysics 312, 1–33. https://doi.org/https://doi.org/10.1016/S0040-1951(99)00169-9

Burnham, C.W., Hiroshi, O., 1980. Late-stage processes of felsic magmatism.

Campos, J.E.G., Dantas, E.L., Roig, H.L., Botelho, N.F., Almeida, T., Souza, V.S., Borges, W.R. (2010), 2010. Projeto Paranã-São Salvador, Tocantins. Brasília.

Chang, Z., Large, R.R., Maslennikov, V., 2008. Sulfur isotopes in sediment-hosted orogenic gold deposits: Evidence for an early timing and a seawater sulfur source. Geology 36, 971–974. https://doi.org/10.1130/G25001A.1

Cordani, U., Sato, K., Teixeira, W., Tassinari, C., Basei, M., 2000. Crustal evolution of the South American platform. Tectonic evolution of South America. Rio de Janeiro 19–40.

Cordani, U.G., Sato, K., 1999. Crustal evolution of the South American Platform, based on Nd isotopic systematics on granitoid rocks. Episodes 22, 167–173. https://doi.org/10.18814/epiiugs/1999/v22i3/003

Cordeiro, P.F. de O., Oliveira, C.G. de, 2017. The Goiás Massif: Implications for a pre-Columbia 2.2–2.0 Ga continent-wide amalgamation cycle in central Brazil. Precambrian Res 298, 403–420. https://doi.org/10.1016/J.PRECAMRES.2017.06.021

Corrêa, R. de S., Oliveira, C.G. de, Vidotti, R.M., Souza, V. da S., 2015. Regional-scale pressure shadow-controlled mineralization in the Príncipe Orogenic Gold Deposit, Central Brazil. Ore Geol Rev 71, 273–304. https://doi.org/https://doi.org/10.1016/j.oregeorev.2015.06.008

Costa, J.B.S., Hasui, Y., 1985. Aspectos lito-estruturais e evolução crustal da região centro-oeste de Goiás (Ph.D. Thesis). Universidade Federal do Pará, Belém.

Cruden, A., Weinberg, R., 2018. Mechanisms of Magma Transport and Storage in the Lower and Middle Crust—Magma Segregation, Ascent and Emplacement, in: Volcanic and Igneous Plumbing Systems. pp. 13–53. https://doi.org/10.1016/B978-0-12-809749-6.00002-9

Cruz, E.L.C.C., 2001. Gênese e o contexto tectônico da mina Córrego Paiol, terreno AlmasConceição: Um depósito de ouro hospedado em anfibolito do embasamento da Faixa de Dobramentos Brasília (Ph.D. Thesis). University of Brasília, Brasília.

Cruz, E.L.C.C., Kuyumjian, R., Boaventura, G., 2003. Low-K calk-alkaline granite series of southeastern Tocantins State: chemical evidence for two sources for the granite-gneissic complexes in the Almas-Dianópolis Terrane. Revista Brasileira de Geociências 33, 125–136. https://doi.org/10.25249/0375-7536.2003332125136

Cruz, E.L.C.C., Kuyumjian, R.M., 1998. The geology and tectonic evolution of the Tocantins granite-greenstone terrane: Almas-Dianópolis region, Tocantins state, central Brazil. Revista Brasileira de Geociências 28, 173–182.

Cuadros, F.A., Botelho, N.F., Fuck, R.A., Dantas, E.L., 2017a. The peraluminous Aurumina Granite Suite in central Brazil: An example of mantle-continental crust interaction in a Paleoproterozoic cordilleran hinterland setting? Precambrian Res 299, 75–100. https://doi.org/https://doi.org/10.1016/j.precamres.2017.07.029

Cuadros, F.A., Botelho, N.F., Fuck, R.A., Dantas, E.L., 2017b. The Ticunzal Formation in central Brazil: Record of Rhyacian sedimentation and metamorphism in the western border of the São Francisco Craton. J South Am Earth Sci 79, 307–325. https://doi.org/https://doi.org/10.1016/j.jsames.2017.08.014

Cunha, L.M., 2006. Gênese e controle da mineralização de Au e Ag associada a granitos peraluminosos na mina de Aurumina, Goiás (Unpublished MSc Thesis). University of Brasília, Brasília.

D'el Rey Silva L.J.H., Senna Filho V., 1998. Ouro em sericita-quartzo hidrotermalitos controlados por cisalhamentos conjugados brasilianos, na região de Cavalcante (GO). Revista Brasileira de Geociências 28, 405–408.

Fernandes, P.E.C.A., Montes, M.L., Braz, E.R.C., Montes, A.S.L., Silva, L.L., Oliveira, F.L.L., Ghignone, J.I., Siga Jr., O., Castro, H.E.F., 1982. Projeto RADAMBRASIL, levantamento de recursos naturais. I - Geologia. Folha SD.23. Brasília.

Fu, Y., Yang, Z., Li, C., Xia, P., 2021. Enrichment of Platinum Group Elements in Lower Cambrian Polymetallic Black Shale, SE Yangtze Block, China. Front Earth Sci (Lausanne) 9.

Fuck, R., 1994. A Faixa Brasília e a compartimentação tectônica na Província Tocantins. SBG, Simpósio de Geologia do Centro-oeste 4, 184–187.

Fuck, R., Neves, B., Schobbenhaus, C., 2008. Rodinia descendants in South America. Precambrian Res 160, 108–126. https://doi.org/10.1016/j.precamres.2007.04.018

Fuck, R.A., Dantas, E.L., Pimentel, M.M., Botelho, N.F., Armstrong, R., Laux, J.H., Junges, S.L., Soares, J.E., Praxedes, I.F., 2014. Paleoproterozoic crust-

formation and reworking events in the Tocantins Province, central Brazil: A contribution for Atlantica supercontinent reconstruction. Precambrian Res 244, 53–74. https://doi.org/10.1016/J.PRECAMRES.2013.12.003

Gaboury, D., 2021. The Neglected Involvement of Organic Matter in Forming Large and Rich Hydrothermal Orogenic Gold Deposits. Geosciences (Basel) 11. https://doi.org/10.3390/geosciences11080344

Goldfarb, R.J., Groves, D.I., 2015. Orogenic gold: Common or evolving fluid and metal sources through time. Lithos 233, 2–26. https://doi.org/https://doi.org/10.1016/j.lithos.2015.07.011

Goldfarb, R.J., Groves, D.I., Gardoll, S., 2001. Orogenic gold and geologic time: a global synthesis. Ore Geol Rev 18, 1–75. https://doi.org/https://doi.org/10.1016/S0169-1368(01)00016-6

Goldfarb, R.J., Pitcairn, I., 2023. Orogenic gold: is a genetic association with magmatism realistic? Miner Depos 58, 5–35. https://doi.org/10.1007/s00126-022-01146-8

Groves, D.I., Goldfarb, R.J., Gebre-Mariam, M., Hagemann, S.G., Robert, F., 1998. Orogenic gold deposits: A proposed classification in the context of their crustal distribution and relationship to other gold deposit types. Ore Geol Rev 13, 7–27. https://doi.org/https://doi.org/10.1016/S0169-1368(97)00012-7

Groves, D.I., Goldfarb, R.J., Robert, F., Hart, C.J.R., 2003. Gold Deposits in Metamorphic Belts: Overview of Current Understanding, Outstanding Problems, Future Research, and Exploration Significance. Economic Geology 98, 1–29. https://doi.org/10.2113/gsecongeo.98.1.1

Groves, D.I., Santosh, M., 2016. The giant Jiaodong gold province: The key to a unified model for orogenic gold deposits? Geoscience Frontiers 7, 409–417. https://doi.org/https://doi.org/10.1016/j.gsf.2015.08.002

Groves, D.I., Santosh, M., Goldfarb, R.J., Zhang, L., 2018. Structural geometry of orogenic gold deposits: Implications for exploration of world-class and giant deposits. Geoscience Frontiers 9, 1163–1177. https://doi.org/https://doi.org/10.1016/j.gsf.2018.01.006

Groves, D.I., Santosh, M., Zhang, L., 2020. A scale-integrated exploration model for orogenic gold deposits based on a mineral system approach. Geoscience Frontiers 11, 719–738. https://doi.org/https://doi.org/10.1016/j.gsf.2019.12.007

Hart, C., 2007. Reduced Intrusion-related Gold Systems, in: Goodfellow W (Ed.), . Geological Association of Canada, Mineral Deposits Division, pp. 95–112.

Hector, S., Patten, C.G.C., Kolb, J., de Araujo Silva, A., Walter, B.F., Molnár, F., 2023. Orogenic Au deposits with atypical metal association (Cu, Co, Ni): Insights from the Pohjanmaa Belt, western Finland. Ore Geol Rev 154, 105326. https://doi.org/https://doi.org/10.1016/j.oregeorev.2023.105326

Holland, H.D., 1979. Metals in black shales; a reassessment. Economic Geology 74, 1676–1680. https://doi.org/10.2113/gsecongeo.74.7.1676

Huston, D., 1999. Stable isotopes and their significance for understanding the genesis of volcanic-hosted massive sulfide deposits: A review. Reviews in Economic Geology 8, 157–179.

Hutchison, W., Finch, A.A., Boyce, A.J., 2020. The sulfur isotope evolution of magmatic-hydrothermal fluids: insights into ore-forming processes. Geochim Cosmochim Acta 288, 176–198. https://doi.org/https://doi.org/10.1016/j.gca.2020.07.042

Ishihara, S., Sasaki, A., 1989. Sulfur isotopic ratios of the magnetite-series and ilmenite-series granitoids of the Sierra Nevada batholith—A reconnaissance study. Geology 17, 788–791. https://doi.org/10.1130/0091-7613(1989)017<0788:SIROTM>2.3.CO;2

Kajiwara, Y., Krouse, H.R., 1971. Sulfur Isotope Partitioning in Metallic Sulfide Systems. Can J Earth Sci 8, 1397–1408. https://doi.org/10.1139/e71-129

Kajiwara, Y., Krouse, H.R., Sasaki, A., 1969. Experimental study of sulfur isotope fractionation between coexistent sulfide minerals. Earth Planet Sci Lett 7, 271–277. https://doi.org/https://doi.org/10.1016/0012-821X(69)90064-8

Kretschmar, U., Scott, S.D., 1976. Phase relations involving arsenopyrite in the system Fe-As-S and their application. The Canadian Mineralogist 14, 364–386.

Kuyumjian, R., Cruz, E., Filho, J., Moura, M., Guimarães, E., Pereira, K., 2012. Geologia e ocorrências de ouro do Terreno Granito-Greenstone do Tocantins, TO: síntese do conhecimento e parâmetros para exploração mineral. Revista Brasileira de Geociências 42, 213–228. https://doi.org/10.25249/0375-7536.2012421213228

LaFlamme, C., Sugiono, D., Thébaud, N., Caruso, S., Fiorentini, M., Selvaraja, V., Jeon, H., Voute, F., Martin, L., 2018. Multiple sulfur isotopes monitor fluid evolution of an Archean orogenic gold deposit. Geochim Cosmochim Acta 222, 436–446. https://doi.org/https://doi.org/10.1016/j.gca.2017.11.003

Lang, J.R., Baker, T., 2001. Intrusion-related gold systems: The present level of understanding. Miner Depos 36, 477–489. https://doi.org/10.1007/s001260100184

Lang, J.R., Baker, T., Hart, C.J.R., Mortensen, J.K., 2000. An exploration model for intrusion-related gold systems. Society of Economic Geologists News 40, 7–15.

Lazarin, M.A., Rabelo, F.C., 1984. Garimpeiros do Nordeste de Goiás, in: Rocha, G.A. (org) (Ed.), Em Busca Do Ouro. Ed. Marco Zero, pp. 107–120.

Mair, J.L., Goldfarb, R.J., Johnson, C.A., Hart, C.J.R., Marsh, E.E., 2006. Geochemical constraints on the genesis of the Scheelite dome intrusion-related gold deposit, Tombstone gold belt, Yukon, Canada. Economic Geology 101, 523–553. https://doi.org/10.2113/gsecongeo.101.3.523

Mair, J.L., Hart, C.J.R., Goldfarb, R.J., O'Dea, M., Harris, S., 2000. Geology and metallogenic signature of gold occurrences at Scheelite Dome, Tombstone gold belt, Yukon.

Marini, O.J., Botelho, N.F., 1986. A província de granitos estaníferos de Goiás. Revista Brasileira de Geociências 16, 119–131.

Marini, O.J., Fuck, R.A., Dardenne, M.A., Danni, J.C.M., 1984. Província Tocantins: setores central e sudeste, in: Almeida, F.F.M., Hasui, Y. (Eds.), O Pré-Cambriano Do Brasil. Edgard Blücher Ltd, pp. 205–264.

Marini, O.J., Liberal, G.S., Dos Reis, L.T., Trinidade, C.A.H., De Souza, S.L., 1978. Nova unidade litoestratigráfica do Pré-Cambriano do estado de Goiás, in: XXX Congresso Brasileiro de Geologia. Boletim 1, Resumos Das Comunicações. Recife, pp. 126–127.

Marsh, E.E., Goldfarb, R.J., Hart, C.J.R., Johnson, C.A., 2003. Geology and geochemistry of the Clear Creek intrusion-related gold occurrences, Tintina Gold Province, Yukon, Canada. Can J Earth Sci 40, 681–699. https://doi.org/10.1139/e03-018

Massucato, A.J., Hippert, J.F.M., 1996. Gold mineralization associated with S-C structures in km-scale extension gashes: the example of Cavalcante-GO., in: XXXIX Congresso Brasileiro de Geologia. Anais SBG 1, Salvador, pp. 343–346.

McDonough, W.F., Sun, S. -s., 1995. The composition of the Earth. Chem Geol 120, 223–253. https://doi.org/https://doi.org/10.1016/0009-2541(94)00140-4

Menez, J., 2014. Depósito não-convencional de ouro, paládio e platina (±urânio) associado a granito peraluminoso, mina buraco do ouro, Cavalcante, Goiás : caracterização e modelo da mineralização (Ph.D. Thesis). University of Brasília, Brasília.

Menez, J., Botelho, N.F., 2017. Ore characterization and textural relationships among gold, selenides, platinum-group minerals and uraninite at the granite-related Buraco do Ouro gold mine, Cavalcante, Central Brazil. Mineral Mag 81, 463–475. https://doi.org/10.1180/minmag.2016.080.101

Meyers, P.A., Pratt, L.M., Nagy, B., 1992. Introduction to geochemistry of metalliferous black shales. Chem Geol 99, vii–xi. https://doi.org/https://doi.org/10.1016/0009-2541(92)90027-3

Miller, C.F., Barton, M.D., 1990. Phanerozoic plutonism in the Cordilleran Interior, U.S.A., in: Kay, S.M., Rapela, C.W. (Eds.), Plutonism from Antarctica to Alaska. Geological Society of America, p. 0. https://doi.org/10.1130/SPE241-p213

Miller, C.F., Stoddard, E.F., Bradfish, L.J., Dollase, W.A., 1981. Composition of plutonic muscovite; genetic implications. The Canadian Mineralogist 19, 25–34.

Moura, M.A., Botelho, N.F., Olivo, G.R., Kyser, K., Pontes, R.M., 2014. Genesis of the Proterozoic Mangabeira tin–indium mineralization, Central Brazil: Evidence

from geology, petrology, fluid inclusion and stable isotope data. Ore Geol Rev 60, 36–49. https://doi.org/https://doi.org/10.1016/j.oregeorev.2013.12.010

Ohmoto, H., 1972. Systematics of Sulfur and Carbon Isotopes in Hydrothermal Ore Deposits. Economic Geology 67, 551–578. https://doi.org/10.2113/gsecongeo.67.5.551

Oliveira, C.G., Vidotti, R.M., Dantas, E.L., Souza, V.S., Chemale, F.J., 2012. Projeto Natividade: Relatório de Graduação do Curso de Geologia da Universidade de Brasília. Brasília (unpublished).

Pagès, A., Barnes, S., Schmid, S., Coveney, R.M., Schwark, L., Liu, W., Grice, K., Fan, H., Wen, H., 2018. Geochemical investigation of the lower Cambrian mineralised black shales of South China and the late Devonian Nick deposit, Canada. Ore Geol Rev 94, 396–413. https://doi.org/https://doi.org/10.1016/j.oregeorev.2018.02.004

Pašava, J., 1993. Anoxic sediments—an important environment for PGE; An overview. Ore Geol Rev 8, 425–445. https://doi.org/https://doi.org/10.1016/0169-1368(93)90037-Y

Petford, N., 2003. Rheology of granitic magmas during ascent and emplacement. Annu. Rev. Earth Planet. Sci 31, 399–427.

Pimentel, M.M., Fuck, R.A., 1992. Neoproterozoic crustal accretion in central Brazil. Geology 20, 375–379. https://doi.org/10.1130/0091-7613(1992)020<0375:NCAICB>2.3.CO;2

Pimentel, M.M., Fuck, R.A., Botelho, N.F., 1999. Granites and the geodynamic history of the neoproterozoic Brasília belt, Central Brazil: a review. Lithos 46, 463–483. https://doi.org/https://doi.org/10.1016/S0024-4937(98)00078-4

Pimentel, M.M., Heaman, L., Fuck, R.A., Marini, O.J., 1991. U-Pb zircon geochronology of Precambrian tin-bearing continental-type acid magmatism in central Brazil. Precambrian Res 52, 321–335. https://doi.org/https://doi.org/10.1016/0301-9268(91)90086-P

Piper, D.Z., 1994. Seawater as the source of minor elements in black shales, phosphorites and other sedimentary rocks. Chem Geol 114, 95–114. https://doi.org/https://doi.org/10.1016/0009-2541(94)90044-2

Poulson, S.R., Ohmoto, H., 1989. Devolatilization equilibria in graphite-pyrite-pyrrhotite bearing pelites with application to magma-pelite interaction. Contributions to Mineralogy and Petrology 101, 418–425. https://doi.org/10.1007/BF00372215

Rimmer, S.M., 2004. Geochemical paleoredox indicators in Devonian–Mississippian black shales, Central Appalachian Basin (USA). Chem Geol 206, 373–391. https://doi.org/https://doi.org/10.1016/j.chemgeo.2003.12.029

Saboia, A.M., Gouveia de Oliveira, C., Dantas, E.L., Scandolara, J.E., Cordeiro, P., Rodrigues, J.B., Cordeiro de Sousa, I.M., 2020. The 2.26 to 2.18 Ga Arc-Related

Magmatism of the Almas-Conceição do Tocantins Domain: An Early Stage of the São Francisco Paleocontinent Assembly in Central Brazil. J South Am Earth Sci 104, 102757. https://doi.org/10.1016/J.JSAMES.2020.102757

Santos, Í.K.M. dos, Souza, V. da S., Botelho, N.F., Hoyer, I. de S., Bonfim, L.A.R., 2023. Mineral chemistry and oxygen isotope studies on Sn (±W) mineralization from Pedra Branca Granite Massif, Central Brazil. Brazilian Journal of Geology 53.

Scharrer, M., Kreissl, S., Markl, G., 2019. The mineralogical variability of hydrothermal native element-arsenide (five-element) associations and the role of physicochemical and kinetic factors concerning sulfur and arsenic. Ore Geol Rev 113, 103025. https://doi.org/https://doi.org/10.1016/j.oregeorev.2019.103025

Seal II, R.R., 2006. Sulfur Isotope Geochemistry of Sulfide Minerals. Rev Mineral Geochem 61, 633–677. https://doi.org/10.2138/rmg.2006.61.12

Serafim, I.C.C.O., 2017. Caracterização Magnética e Gamaespectrométrica de Zonas de Alteração Hidrotermal Associadas à Prospecção Aurífera, Nova Roma e Monte Alegre de Goiás (MSc Dissertation). University of Brasília, Brasília.

Seward, T.M., 1991a. The hydrothermal geochemistry of gold, in: Foster, R.P. (Ed.), Gold Metallogeny and Exploration. Springer US, Boston, MA, pp. 37–62. https://doi.org/10.1007/978-1-4613-0497-5_2

Seward, T.M., 1991b. The hydrothermal geochemistry of gold, in: Foster, R.P. (Ed.), Gold Metallogeny and Exploration. Springer US, Boston, MA, pp. 37–62. https://doi.org/10.1007/978-1-4613-0497-5_2

Sharp, Z.D., Essene, E.J., Kelly, W.C., 1985. A re-examination of the arsenopyrite geothermometer; pressure considerations and applications to natural assemblages. The Canadian Mineralogist 23, 517–534.

Sirqueira, A.R.F., 2014. Rochas albitizadas e albititos relacionados a mineralizações de estanho da Província Estanífera de Goiás: caracterização petrológica e gênese. (MSc Dissertation). University of Brasília, Brasília.

Sousa, I.M.C., Giustina, M.E.S. Della, Oliveira, C.G., 2016. Crustal evolution of the northern Brasília Belt basement, central Brazil: A Rhyacian orogeny coeval with a pre-Rodinia supercontinent assembly. Precambrian Res 273, 129–150. https://doi.org/https://doi.org/10.1016/j.precamres.2015.12.007

Stefánsson, A., Seward, T.M., 2003. The hydrolysis of gold(I) in aqueous solutions to 600°c and 1500 bar. Geochim Cosmochim Acta 67, 1677–1688. https://doi.org/https://doi.org/10.1016/S0016-7037(02)01131-6

Stephens, J.R., Mair, J.L., Oliver, N.H.S., Hart, C.J.R., Baker, T., 2004. Structural and mechanical controls on intrusion-related deposits of the Tombstone Gold Belt, Yukon, Canada, with comparisons to other vein-hosted ore-deposit types. J Struct Geol 26, 1025–1041. https://doi.org/10.1016/j.jsg.2003.11.008

Thompson, J., Sillitoe, R., Baker, T., Lang, J., Mortensen, J., 1999. Intrusion-related gold deposits associated with tungsten-tin provinces. Miner Depos 34, 323–334. https://doi.org/10.1007/s001260050207

Uhlein, A., Fonseca, M., Seer, H., Dardenne, M., 2012. TECTÔNICA DA FAIXA DE DOBRAMENTOS BRASÍLIA – SETORES SETENTRIONAL E MERIDIONAL. Revista Geonomos 2. https://doi.org/10.18285/geonomos.v2i20.243

Woods, A.W., 1992. Melting and dissolving. J Fluid Mech 239, 429–448. https://doi.org/DOI: 10.1017/S0022112092004476

Xu, L., Lehmann, B., Mao, J., 2013. Seawater contribution to polymetallic Ni–Mo–PGE–Au mineralization in Early Cambrian black shales of South China: Evidence from Mo isotope, PGE, trace element, and REE geochemistry. Ore Geol Rev 52, 66–84. https://doi.org/https://doi.org/10.1016/j.oregeorev.2012.06.003

Zheng, Y.-F., Hoefs, J., 1993. Effects of mineral precipitation on the sulfur isotope composition of hydrothermal solutions. Chem Geol 105, 259–269. https://doi.org/https://doi.org/10.1016/0009-2541(93)90130-B

Zhong, R., Brugger, J., Tomkins, A.G., Chen, Y., Li, W., 2015. Fate of gold and base metals during metamorphic devolatilization of a pelite. Geochim Cosmochim Acta 171, 338–352. https://doi.org/https://doi.org/10.1016/j.gca.2015.09.013